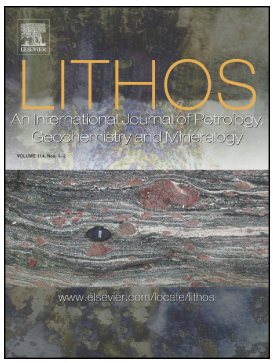


# Origin of the Jurassic-cretaceous intraplate granitoids in Eastern China as a consequence of paleo-Pacific plate subduction

Di Hong, Yaoling Niu, Yuanyuan Xiao, Pu Sun, Juanjuan Kong, Pengyuan Guo, Fengli Shao, Xiaohong Wang, Meng Duan, Qiqi Xue, Hongmei Gong, Shuo Chen

PII: S0024-4937(18)30392-X
DOI: doi:10.1016/j.lithos.2018.10.027
Reference: LITHOS 4843

To appear in: *LITHOS*

Received date: 6 August 2018
Accepted date: 23 October 2018

Please cite this article as: Di Hong, Yaoling Niu, Yuanyuan Xiao, Pu Sun, Juanjuan Kong, Pengyuan Guo, Fengli Shao, Xiaohong Wang, Meng Duan, Qiqi Xue, Hongmei Gong, Shuo Chen , Origin of the Jurassic-cretaceous intraplate granitoids in Eastern China as a consequence of paleo-Pacific plate subduction. Lithos (2018), doi:10.1016/j.lithos.2018.10.027

# Origin of the Jurassic-Cretaceous intraplate granitoids in Eastern China as a consequence of paleo-Pacific plate subduction

Di Hong [a, b, c*], Yaoling Niu [a, b, d, e*], Yuanyuan Xiao [a, b], Pu Sun [a, b], Juanjuan Kong [a, b, c], Pengyuan Guo [a, b], Fengli Shao [f], Xiaohong Wang [a, b], Meng Duan [e], Qiqi Xue [e], Hongmei Gong [a, b], Shuo Chen [a, b]

[a] Institute of Oceanology, Chinese Academy of Sciences, Qingdao 266071, China

[b] Laboratory for Marine Geology, Qingdao National Laboratory for Marine Science and Technology, Qingdao 266061, China

[c] University of Chinese Academy of Sciences, Beijing 100049, China

[d] Department of Earth Sciences, Durham University, Durham DH1 3LE, UK

[e] School of Earth Science and Mineral Resources, China University of Geosciences, Beijing 100083, China

[f] Linyi University, Institute of Geology and Paleontology, Linyi 276000, China

***Corresponding authors.**

E-mail addresses: hd_ice@live.com (D. Hong), yaoling.niu@durham.ac.uk (Y. Niu)

## Abstract

Jurassic-Cretaceous granitoids are widespread in eastern continental China and have been considered by many as resulting from paleo-Pacific subduction. However, the actual mechanism of their petrogenesis remains speculative. In order to address this important problem and on the basis of our regional study, we hypothesized that the coastal granitoids may result directly from the paleo-Pacific plate subduction, whereas the widespread granitoids in the continental interiors ultimately result from dehydration of the paleo-Pacific slab stagnated in the mantle transition zone (Niu et al., 2015). Here, we present the very first study testing this hypothesis. We sampled 18 Jurassic-Cretaceous granitoid plutons along a ~ 1300 km long traverse parallel to the inferred paleo-Pacific subduction from the southeast coastline to the Xiaoqinling in the continental interiors and carried out a detailed study on these plutonic samples, including zircon U-Pb geochronology, bulk-rock major and trace element compositions and Sr-Nd-Pb-Hf isotopic characteristics. These plutons give varying zircon crystallization ages of ~146 to 100 Ma. They are mostly granitic and minor granodioritic, quartz monzonitic and syenitic in composition, enriched in large ion lithophile elements (LILEs), depleted in high field-strength elements (HFSEs) and have varying negative Sr and Eu anomalies. The plutons in the continental interiors show significant positive correlations of Nd ($\varepsilon_{Nd}$ (t) = -25.5 to -10.9) and Hf ($\varepsilon_{Hf}$ (t) = -31.5 to -11.3) isotopes with Pb isotopes ($^{206}Pb/^{204}Pb$ (t) = 15.827 to 17.622), with the enriched endmember characterized by low $\varepsilon_{Nd}$ (t), $\varepsilon_{Hf}$ (t) and $^{206}Pb/^{204}Pb$ (t). The

plutons towards the coastal region have relatively high $\varepsilon_{Nd}$ (t) (-9.0 to -5.2), $\varepsilon_{Hf}$ (t) (-11.2 to -4.1) and $^{206}Pb/^{204}Pb$ (t) (18.051 to 18.349). The coastal granitoids are best explained as resulting directly from subduction slab dehydration induced mantle wedge melting and resultant crustal anatexis, whereas the interior granitoids are best interpreted as resulting from mature crustal anataxis caused by basaltic magmatism associated with mantle lithosphere thinning, ultimately triggered by dehydration of paleo-Pacific slab stagnant in the mantle transition zone.

**Key words:** Jurassic-Cretaceous granitoids in eastern China; Lithosphere thinning; Basal hydration weakening; Paleo-Pacific plate subduction; Crustal melting

## 1. Introduction

Jurassic–Cretaceous granitoids are widespread in eastern continental China (from Northeast China to North China and to Southeast China and are distributed randomly in a wide zone in excess of 1000 km (Fig. 1). Of particular interest are series of granitoid plutons forming an apparent linear chain of NW-SE trending located north of the Qinling-Dabie Orogen, extending to the Xiaoqinling (Fig. 1) further to the west because of exhumation and outcropping in response to the continued South-North China converge since the Mesozoic (Niu et al., 2015). This plutonic “chain” offers a prime opportunity to study the petrogenesis of these granitoids in time (varying ages) and space (distance to the coastal line). These granitoids were traditionally considered to have emplaced during the “Yanshanian” magmatic event. The isotopic age data,

however, indicate two separate events of 190–150 and 140–85Ma (Li, 2000; Wu et al., 2005a, 2005b), defining the early and late Yanshanian granitoid magmatism. The origin of the Jurassic-Cretaceous granitoids remains under debate. There are four major models (1) slab-tearing during paleo-Pacific subduction (Wu et al., 2012); (2) crust-mantle interaction in an extensional setting, due to lithospheric thinning caused by westward subduction of the paleo-Pacific plate (Gao et al., 2014); (3) crustal remelting/ anataxis during post-collisional compression-extension transition and the back-arc extension related to paleo-Pacific subduction (e.g., Zhou et al., 2006; Li et al., 2018); (4) upwelling of the asthenospheric mantle, causing crustal melting due to a slab break-off and rollback of the subducting paleo-Pacific Plate (Li et al., 2014). Based on the analysis of the distribution of Mesozoic granitoids in eastern continental China in space and time, Niu et al. (2015) hypothesized that the process of basal hydration weakening that weakens and converts the basal lithosphere into asthenosphere while producing basaltic melts from the being-converted mantle lithosphere, which rise and underplate, causing crustal melting for these Jurassic-Cretaceous granitoids in the continental interiors. However, the granitoids in the coastal region must have directly resulted from the paleo-Pacific subduction before the trench jam and subduction cessation at ~ 100 Ma (Niu et al., 2015).

The role of paleo-Pacific subduction is now widely accepted, but the exact mechanism of the granitoid magmatism remains unclear. With all these different views objectively considered, the hypothesis by Niu et al. (2015) is geologically testable. The ~ 1300 km long plutonic “chain”, that is parallel to and located north of,

the older (~ 230 Ma) Qinling-Dabie Orogen offers a test ground. We understand that this apparent linear granitoid chain does not represent the expected areal distribution of the granitoids in eastern continental China but results from preferential exhumation and exposure because of continued South-North China convergence since the Mesozoic, as evidenced by the ~ 400 km offset along the sinistral Tan-Lu fault (Niu et al., 2015).

To test the hypothesis, we sampled 18 granitoid plutons along the "chain" (Fig. 1), and carried out detailed zircon U-Pb geochronology, bulk-rock major and trace element analysis and Sr-Nd-Pb-Hf isotopic geochemistry on representative samples of the 18 plutons.

## 2. Geological setting and petrography

### 2.1 Geological background

The eastern continental China includes the Northeast (NE) China and North China Craton (NCC) in the north, the Qinling-Dabie Orogen in the middle, and the South China Block (SCB) in the south (Fig. 1). NE China is located in the eastern segment of the Central Asian Orogenic Belt and is generally considered to be a tectonic collage of several microcontinental blocks (Jahn et al., 2000a, b, 2004; Windley et al., 2007; Li et al., 2013). The NCC is one of the oldest cratons in the world with an earliest record of > 3.8 Gyrs (Jahn et al., 1987; Liu et al., 1992), and can be divided into West Block (WB), East Block (EB) and Trans-North China Orogen (TNCO) based on ages, lithological assemblage, geochemistry and

metamorphic history of basement rocks (Zhao et al., 2001; Fig. 1). The Qinling-Dabie Orogen represents the most important SCB-NCC continental collision largely completed in the Late Triassic (Fig. 1, Mattauer et al., 1985; Sengör, 1985; Hsü et al., 1987; Zhang, 1985). The SCB can be further divided into the Yangtze (YZ) Craton to the northwest and the Cathaysia Block (CB) to the southeast (Fig. 1). It is generally considered that the amalgamation of the Yangtze Craton and Cathaysia Block took place during the Late Mesoproterozoic at ~0.9 Ga associated with the supercontinent Rodinia amalgamation (Li et al., 2009). The Xiaoqinling granitoid "chain" is located at the southern margin of the NCC, immediately north of the Qinling-Dabie Orogen (Fig. 1), intruding the Neoarchaean to Palaeoproterozoic amphibolite- to granulite-facies metamorphic basement of the Taihua Group dominated by amphibolite with varying amounts of biotite plagioclase gneiss, migmatite, quartzite, and marble.

However, a detailed analysis of the Jurassic-Cretaceous granitoid magmatism throughout eastern continental China shows random distribution in space and time with no recognizable trends in a wide W-E zone in excess of 1000 km (Niu et al., 2015). This leads to the hypothesis that the stagnant paleo-Pacific slab in the mantle transition zone beneath the region dehydrated and released water in the form of hydrous melt that percolated through and metasomatized the upper mantle, weakened the base of the lithosphere while producing basaltic melt as the heat source (also material contribution) for crustal melting and the granitoid magmatism (Niu et al., 2015).

### 2.3 Petrography

The 18 Jurassic-Cretaceous (106.2 – 154 Ma) granitoid plutons (GPS data are given in Table 2) crop out along a traverse of ~ 1300 km and over an area of ~10 to 784 $km^2$ (Table 1). The granitoids are mainly granitic with minor syenitic, quartz monzonitic and granodioritic compositions (Table 2) with varying grain size (Fig. 2). The mineralogy is simple, dominated by plagioclase (30-42%), K-feldspar (30-38%), quartz (20-30%), biotite (5%) and minor amphibole (2-10%) (Fig. 2). Accessory minerals include apatite, zircon, and Fe-Ti oxides. The petrographic detail is given in Table 2.

## 3. Analytical methods

### 3.1. Zircon U-Pb dating

Nine samples were selected for zircon U-Pb dating. Zircon LA-ICP-MS U–Pb dating was carried out at the Laboratory of Ocean Lithosphere and Mantle Dynamics, Institute of Oceanology, Chinese Academy of Sciences (IOCAS). Laser sampling was performed using a Photon Machines Excite 193 nm excimer laser system. An Agilent 7900 Inductively Coupled Plasma Mass Spectrometer (ICP-MS) instrument was used to acquire ion-signal intensities. Spot diameter was set 35 μm. Zircon 91500 was used as external standard for U-Pb dating (Wiedenbeck et al., 1995), and analyzed twice between every 5 unknown analyses. The standard silicate glass NIST SRM610 was used to calibrate U, Th and Pb concentrations. The analytical detail is given in Xiao et

al. (unpublished).

### 3.2. Major and trace elements

Bulk-rock major elements were analysed using an Inductively Coupled Plasma Optical Emission Spectroscopy (ICP-OES, Agilent 5100) in the IOCAS. The replicate sample was used to monitor precisions (<5.0%, see Appendix A). The USGS standard STM-2, RGM-2, W-2 and the replicate sample were used to monitor the analytical accuracy (±5%, see Appendix B) and precision (1σ, <2.0%). The analytical detail is given in Kong et al. (in preparation). Trace elements were analysed using an ICP-MS (Agilent 7900) after total acid digestion in Teflon bombs and dilution. The replicate sample was used to monitor precisions (<5.0%, see Appendix A). Repeated analyses of USGS reference rock standards BCR-2, BHVO-2, AGV-2, RGM-2 and GSP-2 give analytical precision better than 5% and accuracies better than 10% for all elements but Be (12%). The analytical detail is given in Chen et al. (2017). The analytical results are given in Appendix C.

### 3.3. Sr-Nd-Pb-Hf isotopes

Sr-Nd-Pb-Hf isotopes were measured using Nu Plasma Multi-Collector Inductively Coupled Plasma Mass Spectrometry (MC-ICP-MS) at the Radiogenic Isotope Facility at The University of Queensland, Australia (UQ). Analytical details for sample digestion and Sr-Nd-Pb-Hf elemental separation are given in Guo et al. (2014) and Sun et al. (2017). The measured $^{87}Sr/^{86}Sr$, $^{143}Nd/^{144}Nd$ and $^{179}Hf/^{177}Hf$ isotope ratios were corrected for instrumental mass fraction using the exponential law

to $^{86}Sr/^{88}Sr$ = 0.1194, $^{146}Nd/^{144}Nd$ = 0.7219, $^{179}Hf/^{177}Hf$ = 0.7325, respectively. The measured average value for NBS-987 Sr standard is $^{87}Sr/^{86}Sr$ = 0.710249 ± 15 (n = 34, 2σ), identical to measured using TIMS within error ($^{87}Sr/^{86}Sr$ = 0.710250 ± 11 (n = 15, 2σ)). The Nd metal 50ppb, an in-house Nd standard, gives an average $^{143}Nd/^{144}Nd$ of 0.511966 ± 6 (n = 21, 2σ). The repeated measurement of Hf standard (40 ppb) gives an average $^{176}Hf/^{177}Hf$ value of 0.282145 ± 6 (n = 14, 2σ). Pb isotope ratios were normalized for instrumental mass fraction relative to NBS/SRM 997 $^{203}Tl/^{205}Tl$ = 0.41891, which were then normalized against NBS981 (analyzed as a bracketing standard every six samples; White et al., 2000) using $^{206}Pb/^{204}Pb$ = 16.9410, $^{207}Pb/^{204}Pb$ = 15.4944, and $^{208}Pb/^{204}Pb$ = 36.7179 (Collerson et al., 2002). The Geological Survey of Japan (GSJ) rock reference sample JG-3 and the U.S. Geological Survey (USGS) rock standard BCR-2 were repeatedly measured along with our samples, which were consistent with the reference values (GeoReM, http://georem.mpch-mainz.gwdg.de/). See Appendix D for Sr-Nd-Pb-Hf isotope analytical results of the GSJ and USGS reference materials JG-3 and BCR-2, and they are within the recommended values.

Given the significant positive correlations of Nd, Hf isotopes with Pb isotopes of the interior granitoids (see below), we reanalysed five samples (LN14-09, MGS14-02, BMJ14-01, SC14-02, LNS14-03) at the IOCAS using Nu Plasma II MC-ICP-MS to verify the Sr-Nd-Pb-Hf isotope data obtained from UQ are fully reproducible (see Table 3 and Appendix F). Analytical details for sample digestion and Sr-Nd-Pb-Hf elemental separation are given in Sun et al. (unpublished). The measured $^{87}Sr/^{86}Sr$,

$^{143}Nd/^{144}Nd$ and $^{176}Hf/^{177}Hf$ isotope ratios were normalized for instrumental mass fraction using the exponential law to $^{86}Sr/^{88}Sr = 0.1194$, $^{146}Nd/^{144}Nd = 0.7219$ and $^{179}Hf/^{177}Hf = 0.7325$, respectively. International standards of NBS-987, JNdi-1 and Alfa Hf were used as bracketing standards every five samples to monitor the instrument drift during the analysis of Sr, Nd and Hf isotopes, respectively. Repeated analysis for NBS-987 gives an average $^{87}Sr/^{86}Sr = 0.710250 \pm 22$ (n=4, 2σ). Repeated analysis for JNdi-1 gives an average $^{143}Nd/^{144}Nd = 0.512089 \pm 5$ (n=3, 2σ), and repeated analysis for Alfa Hf gives an average $^{176}Hf/^{177}Hf = 0.282198 \pm 9$ (n=5, 2σ). Pb isotope ratios were normalized for instrumental mass fraction relative to NBS/SRM 997 $^{203}Tl/^{205}Tl = 0.41891$. The international standard NBS-981 was used to monitor the instrument drift during the analysis of Pb isotopes. Repeated analysis of NBS-981 gives average $^{206}Pb/^{204}Pb = 16.934 \pm 0.002$ (n = 4, 2σ), $^{207}Pb/^{204}Pb = 15.493 \pm 0.003$ (n = 4, 2σ), and $^{208}Pb/^{204}Pb = 36.689 \pm 0.007$ (n = 4, 2σ). Analytical results of the USGS reference material AGV-2 and GSP-2 are summarized in Appendix D, and they are within the recommended values.

## 4. Data

### 4.1. Zircon U-Pb ages

The results of the U-Pb dating are given in Appendix E and shown in Fig. 3. These zircons are transparent, euhedral, prismatic crystals and have regular oscillatory magmatic zoning (Fig. 3). They have varying Th (67 to 3352 ppm) and U (167 to 2288 ppm) contents with Th/U ratios of 0.39 to 3.51. They give weighted mean

crystallization ages varying from 99.2 ± 2.0 to 146.7 ± 2.3 Ma (Fig. 3).

### 4.2. Major and trace elements

Major and trace element data are given in Appendix A. As shown in the TAS diagram (Fig. 4), these granitoids are dominated by granite with minor syenite, quartz monzonite and granodiorite, which is consistent with the petrography. These granitoids show rough negative trends in $SiO_2$-variation diagrams (Fig. 5), especially $TiO_2$, $Al_2O_3$, $^{T}Fe_2O_3$ and CaO, which likely reflecting varying extents of fractional crystallization although these plutons and samples do not share a common lineage because their emplacement differ in time and space and because they do not show correlated trends for $P_2O_5$, Zr, Sr and Eu/Eu*. In the primitive mantle normalized multi-element diagram (Fig. 6), all the samples show spikes of some large ion lithophile elements (LILE; e.g., Rb, Th, U, K, Pb) and troughs of high field-strength elements (HFSE; e.g., Ni, Ta, Ti, P), resembling the pattern of the bulk continental crust (BCC; Rudnick and Gao, 2003).

### 4.3. Sr-Nd-Pb-Hf isotopes

The bulk-rock Sr-Nd-Pb-Hf isotopic data are given in Table 3 and shown in Fig. 7. The initial Sr-Nd-Pb-Hf isotope ratios were calculated using the zircon U-Pb ages. These granitoids have moderately high initial $^{87}Sr/^{86}Sr$ ratios (0.7076 to 0.7091), relatively low $\varepsilon_{Nd}(t)$ (-3.1 to -22.6) and $\varepsilon_{Hf}(t)$ (-4.1 to -31.5), and varying Pb isotopes ($^{208}Pb/^{204}Pb)_t$ = 36.948 to 38.720, ($^{207}Pb/^{204}Pb)_t$ = 15.22 to 15.646, ($^{206}Pb/^{204}Pb)_t$ = 16.216 to 18.349. They plot to the left of the north-hemisphere reference line (NHRL)

(Fig. 7). Our samples have positive correlation between Nd and Hf isotopes as expected (Vervoort and Blichert-Toft 1999, Vervoort et al., 2011), but unexpectedly positive correlations of Nd and Hf isotopes with Pb isotopes for granitoids in the continental interiors in terms of magmatic processes recorded in the sources and source histories (Fig. 7). These correlations reflect a two-component mixing process of the plutons in the continental interiors, with the enriched endmember and the less enriched endmember (Fig. 7, $\varepsilon_{Nd}$ (t) (-25.5 to -10.9), $\varepsilon_{Hf}$ (t) (-31.5 to -11.3) and $^{206}Pb/^{204}Pb$ (t) = (15.827 to 17.622)). In contrast, the coastal granitoids have high $\varepsilon_{Nd}$ (t) (-9.0 to -5.2), $\varepsilon_{Hf}$ (t) (-11.2 to -4.1) and $^{206}Pb/^{204}Pb$ (t) (18.051 to 18.349).

The lower continental crust from the Dabie, the North China Craton, the Northern Qinling, the south margin of the North China Craton, Yangzi Craton and Cathaysia Block are characterized by high initial $^{87}Sr/^{86}Sr$ ratios, low $\varepsilon_{Nd}$ (t) and $^{206}Pb/^{204}Pb$ (t), which differs from those of the coastal granitoids (Fig. 7). Thus, their differences cannot cause the isotopic differences of the plutons in the continental interiors, as well as the distinct Sr-Nd-Pb-Hf isotopic values between the coastal granitoids and the interior granitoids.

## 5. Discussion

### 5.1 Origin of the interior granitoids

Isotopically, the two-component mixing for the interior granitoids provide clues on their petrogenesis. The lower continental crust is characterized by low U/Pb, Th/Pb, Sm/Nd and Lu/Hf and high Rb/Sr elemental ratios (Fig. 6; Rudnick and Gao, 2003)

relative the primitive mantle (Sun and McDonough, 1989) and will develop, with time, unradiogenic Nd (low $\varepsilon_{Nd}(t)$), Hf (low $\varepsilon_{Hf}(t)$) and Pb (low $^{206}Pb/^{204}Pb$ (t), $^{208}Pb/^{204}Pb$ (t)), and relatively radiogenic Sr (high $^{87}Sr/^{86}Sr(t)$). Therefore, the mature lower continental crust is most likely the enriched isotopic endmember of the two-component mixing. This enriched component is isotopically equivalent to the EM1-like (enriched mantle I) endmember, which is indeed characteristic of the lower crust as revealed through isotopic studies of the lower crustal xenoliths (e.g., Liu et al., 2004; Zhou et al., 2002). This observation supports the hypothesis of mature lower continental crust melting for the granitoids (Niu et al., 2015).

Melting of the mature lower continental crust requires heat and such heat can only be made available by volumetrically significant mantle-derived basaltic melts that underplate/intrude the deep crust (Niu, 2005). This is indeed the case beneath eastern continental China in the Mesozoic because of the widespread lithosphere thinning throughout entire eastern China (Niu, 2005, 2014; Niu et al., 2015), with the intense lithosphere thinning taking place beneath the North China Craton (NCC) from ~ 200 km in the late Paleozoic to the present-day thin lithosphere of ~ 80 km or less (e.g., Menzies 1993; Deng et al., 1998; Griffin et al. 1998; Xu, 2001; Gao et al., 2002, 2004; Yang 2003; Zhu et al., 2012). There are several ideas on the lithosphere thinning, including lithosphere delamination (Menzies, 1993; Deng et al., 1998; Griffin et al. 1998; Xu, 2001; Gao et al., 2004), mantle plume heating (Deng et al., 1998), thermal and chemical metasomatism/erosion (Griffin et al., 1998; Zhang et al., 2003, 2004), and paleo-Pacific plate subduction (Niu, 2005, 2006, 2009; Zhu et al.,

2012, 2013), but physically the most likely mechanism is the basal hydration weakening by converting the basal portions of the lithosphere (i.e., sub-continental lithospheric mantle or SCLM) into the asthenosphere accompanied by partial melting and basaltic magmatism (Niu, 2005, 2006, 2009, 2014; Niu et al., 2015). The water required for such dehydration weakening originated from the paleo-Pacific plate lying stagnantly in the mantle transition zone (Niu, 2005, 2014). The ascent, intruding and underplating of the basaltic magmas provides the heat for the widespread crustal melting for the granitoid magmatism (Niu et al., 2015). Tomographic images beneath eastern China shows that the cold, flat slabs distribute widely throughout eastern China within the mantle transition zone (Zhao et al., 2004), suggesting that melting of the subducted slab was limited and cannot produce voluminously basaltic melts. Thus, the basal portions of the SCLM is the very source of these basaltic melts, rather than the stagnated subducting slabs.

It is conceptually important to note, however, that the heat for the crustal melting is carried by the SCLM-derived basaltic melts and such melts thus have material contribution to the granitoid magmatism. This is indeed the case as evidence in the isotope spaces, especially those involving Pb isotopes (Fig. 7; also see below).

Because of the metasomatic histories of the SCLM, its basaltic magmas are expected to have more enriched Sr-Nd-Hf isotopes (e.g., lower Nd, Hf and higher Sr isotope values) than the DMM (depleted MORB mantle) but would still have less enriched Nd-Hf-Sr isotopes than the LCC (mature lower continental crust), which is expected to have relatively unradiogenic Pb isotopes as discussed above (Zhang et al.,

2002, 2003; Guo et al., 2014). The interior granitoids plot in the field between the LCC and the SCLM (Fig. 7), suggesting that they are isotopic endmembers for the interior granitoids. Therefore, the widespread Jurassic-Cretaceous granitoids in eastern China result from crustal melting induced by basaltic melts derived from partial melting of the SCLM that was undergoing dehydration weakening and thinning (Niu et al., 2015).

Importantly, we recognize a systematic Nd-Hf-Pb isotope ratio increase for the interior granitoids from the coastline to the continental interior (Fig. 8), pointing to the increasing SCLM-over-LCC source contribution to the granitoids.

**5.2 Origin of the coastal granitoids**

Many studies consider that the Jurassic-Cretaceous granitoids along the southeast coastline resulted from paleo-Pacific subduction (e.g., Zhou et al., 2006; Niu et al., 2015). The present-day trench is hundreds of kilometers away from the southeastern coastline. However, the isotopic features of these coastal granitoids indicate that they were produced in a subduction zone setting. We suggest that our geochemical observations support the hypothesis that in the Mesozoic when these 'coastal granitoids' formed, the southeastern coastline of SE China was the location of the trench (see Fig.1, Niu et al., 2015).

Fig. 7 and Fig. 8 show that the coastal granitoids differ distinctly from those of the continental interiors by having high Nd-Hf-Pb isotopes, indicating greater asthenospheric mantle (and less crustal) contribution. The coastal granitoids plot in

the field between the DMM and the SCLM (Fig. 7), suggesting that the underplated basaltic melts must have come from a mantle wedge environment, isotopically resembling basalts and granitoids from subduction settings such as Andean-type continental margin and western Pacific island arcs (Fig. 7). That is, the petrogenesis of the coastal granitoids are more directly related to the active subduction of the paleo-Pacific plate with the mantle wedge derived basaltic melts (the more depleted endmember) intruding/underplating the overlying crust, producing the observed coastal granitoids.

**5.3 Geodynamic significance**

The granitoids in the continental interiors of eastern China are distributed in a wide zone in excess of > 1000 km (Fig. 1, Fig. 8 and Fig. 9), indicating that the Mesozoic lithosphere thinning was not limited to the NCC, but took place throughout the entire eastern continental China as illustrated by Niu (2005) and Niu et al. (2015). This understanding also supports the proposal that the eastern continental China was not an Andean-type margin in the Jurassic-Cretaceous because of lacking a well-defined narrow continental magmatic arc as does along the Andes at present (Niu et al., 2015).

What may have caused the lithospheric thinning and the extensive granitoid magmatism in the Jurassic-Cretaceous Mesozoic? (1) Lithosphere stretching induced asthenosphere upwelling can be ruled out because there are no stretching-related linear magmatism in eastern continental China; (2) thermal mantle plume melting can

be ruled out also because of lacking flood basalts, lacking expected space-time pattern of surface magmatism, and because plume melting residues would thicken, not thin, the lithosphere against geological record (Niu et al., 2015); (3) the delamination model can also be ruled out because it is physically not plausible how buoyant SCLM sinks into the dense asthenosphere in such a wide zone (in excess of > 1000 km). Some previous studies proposed that these granitoids have something to do with the post-collisional processes (e.g., Wang et al., 2013) associated with the collision of the South China Block and the North China Craton in the Late Triassic (242-219 Ma, Ames et al., 1993; Li et al., 1993; Okay and Sengör, 1993; Hacker et al., 1996; Zhang et al., 1996; Wan et al., 2005; Liu et al., 2006; Zhao et al., 2006, 2007; Duan et al., 2016; Kong et al., 2017). However, our studied plutons have distinct emplacement time of ~146 to 100 Ma and it is physically and geologically unlikely that these granitoids would have been caused by the continental collision taking place over some ~ 100 Myrs earlier.

Theoretically, there are three basic mechanisms through which a solid rock can partially melt to form magmas: (1) heating; (2) decompression and; (3) water (plus other possible fluids) addition (Niu, 2005). We have precluded the mechanisms of heating (thermal mantle plume melting) and decompression (lithosphere stretching induced asthenosphere upwelling). Thus, water addition is the most likely mechanism that results in lithospheric mantle melting and induced crustal melting. Niu (2005) and Niu et al. (2015) proposed that the basal hydration weakening concept is the common cause resulting in the lithosphere thinning, lithospheric mantle melting and induced

crustal melting. This concept is supported by the random distribution of the granitoids in space and time in the continental interiors in a wide zone in excess of > 1000 km, contrary to the arguments and ideal model expectation in the literature that there is a systematic NW-to-SE granitoid age decrease, which actually does not exist (see Fig. 9, Niu et al., 2015). In the Mesozoic, the source of water or ‘‘water reservoir’’ was most probably the stagnant paleo-Pacific slab in the mantle transition zone that laterally extended far to the west in excess of 1000 km from the coast as is the case observed in the Cenozoic (Karason and Hilst 2000; Zhao and Ohtani 2009). Water released from the stagnated slab in the form of hydrated melts that rises, weakens and converts the basal lithosphere into asthenosphere while producing basaltic melts from the being-converted mantle lithosphere. These basaltic melts rise, underplate and intrude the crust causing mature crustal melting to form the voluminous Jurassic-Cretaceous granitoids in the interiors of eastern continental China. This concept is illustrated schematically in Fig. 10. Therefore, the interior granitoids were formed in the intra-plate setting rather than an active subduction setting nor post-collisional products of the ~ 220 Ma Qinling-Dabie Orogen as interpreted by some.

## 6. Summary

(1) The Jurassic-Cretaceous granitoids (~ 146 - 100 Ma) in the interiors of eastern continental China (e.g., Xiaoqinling area) have distinct isotopic compositions from those of coastal granitoids, indicating their different sources and petrogenesis.

(2) The interior granitoids show isotopically two-component mixing trends with the

"enriched endmember" well represented by the LCC (mature lower continental crust) because they both consistently have high radiogenic Sr, and low radiogenic Nd-Hf-Pb isotopes. The "depleted" or "less enriched" endmember is best represented by the SCLM (metasomatized mantle lithosphere) (Fig. 7).

(3) We conclude from "(2)" above that the interior granitoids result from partial melting of the LCC, triggered by underplating/intruding of basaltic melts derived from the SCLM undergoing basal hydration weakening and lithosphere thinning (Niu, 2005; Niu et al., 2015).

(4) The coastal granitoids show higher radiogenic Nd-Hf-Pb isotopes, approaching isotopic compositions of basalts and granitoids from subduction settings such as the Andean-type continental margin and western Pacific island arcs. That is, the coastal granitoids are best interpreted as resulting directly from subduction slab dehydration induced mantle wedge melting and resultant crustal anatexis. This offers material evidence supporting the proposal for the exotic origin of Chinese continental shelf (Niu et al., 2015).

## Acknowledgements

We thank Yu Zhang, Yan Hu and Zhenxing Hu for field sampling and sample preparation. We thank Jiyong Li and Dr. Bruno Dhuime for their constructive advices during this research. This work was supported by Marine Geological Process and Environment (U1606401), NSFC (grants: 41630968), Chinese Academy of Sciences (Innovation Grant Y42217101L) and the 111 Project of China (B118048).

## References:

Ames, L., Tilton G. R., Zhou, G. Z., 1993. Timing of collision of the Sino-Korean and Yangtse cratons: U–Pb zircon dating of coesite-bearing ecologites. Geology, 21, 339–342.

Béguelin, P., Chiaradia, M., Beate, B., Spikings, R., 2015. The yanaurcu volcano (western cordillera, ecuador): a field, petrographic, geochemical, isotopic and geochronological study. Lithos, 218-219, 37-53.

Beccaluva, L., 1980. Geochemistry and K/Ar ages of volcanics dredged in the philippine sea (mariana, yap, and palau trenches and parece vela basin). the tectonic and geologic evolution of southeast asian seas and islands. Geophys Monogr, 23.

Chiaradia, M., 2004. Metal sources in mineral deposits and crustal rocks of ecuador (1 N-4 S): a lead isotope synthesis. Economic Geology, 99(6), 1085-1106.

Chiaradia, M., Fontboté, L., Beate, B., 2004. Cenozoic continental arc magmatism and associated mineralization in ecuador. Mineralium Deposita, 39(2), 204-222.

Chiaradia, M., Barnes, J. D., Cadet-Voisin, S., 2014. Chlorine stable isotope variations across the quaternary volcanic arc of ecuador. Earth Planetary Science Letters, 396(396), 22-33.

Chen, J., Jahn, B. M., 1998. Crustal evolution of southeastern china: Nd and Sr isotopic evidence. Tectonophysics, 284(1–2), 101-133.

Chen, S., Wang, X.H., Niu, Y.L., Sun, P., Duan, M., Xiao, Y.Y., Xue, Q.Q., 2017.

Simple and cost-effective methods for precise analysis of trace element abundances in geological materials with ICP-MS. Science Bulletin, 62, 277-289.

Collerson, K.D., Kamber, B.S., Schoenberg, R., 2002. Applications of accurate, highprecision Pb isotope ratio measurement by multi-collector ICP-MS. Chemical Geology, 188, 65-83.

Crawford, A. J., Beccaluva, L., Serri, G., Dostal, J., 1986. Petrology, geochemistry and tectonic implications of volcanics dredged from the intersection of the yap and mariana trenches. Earth Planetary Science Letters, 80(3), 265-280.

Davidson, J. P., Silva, S. L. D., 1995. Late Cenozoic magmatism of the bolivian altiplano. Contributions to Mineralogy Petrology, 119(4), 387-408.

Deng, J., Zhao, H., Luo, Z., 1998. Mantle plumes and lithosphere motion in east Asia. Am Geophys Union Geodyn Ser, 27, 59-66.

Duan, M., Niu, Y.L., Kong, J.J., Sun, P., Hu, Y., Zhang, Y., Chen, S., Li, J.Y., 2016. Zircon U-Pb geochronology, Sr-Nd-Hf isotopic composition and geological significance of the Late-Triassic Baijiazhuang and Lvjing granitic plutons in western Qinling Orogen. Lithos, 260, 443-456.

Dufrane, S. A., Asmerom, Y., Mukasa, S. B., Morris, J. D., Dreyer, B. M., 2006. Subduction and melting processes inferred from u-series, Sr–Nd–Pb isotope, and trace element data, bicol and bataan arcs, philippines. Geochimica Et Cosmochimica Acta, 70(13), 3401-3420.

Ewart, A., Brothers, R. N., Mateen, A., 1977. An outline of the geology and geochemistry, and the possible petrogenetic evolution of the volcanic rocks of

the Tonga-Kermadec-New Zealand island arc. Journal of Volcanology Geothermal Research, 2(3), 205-250.

Elliott, T., Plank, T., Zindler, A., White, W., Bourdon, B., 1997. Element transport from slab to volcanic front at the Mariana arc. Journal of Geophysical Research Solid Earth, 102(B7), 14991-15019.

Gao, S., Rudnick, R.L., Carlson, R.W., McDonough, W.F., Liu, Y.S., 2002. Re–Os evidence for replacement of ancient mantle lithosphere beneath the North China craton. Earth Planet Sci Lett, 198, 307–322.

Gao, S., Rudnick, R. L., Yuan, H. L., Liu, X. M., Liu, Y. S., Xu, W. L., John Ayers., Wang, X. C., Wang, Q. H., 2004. Recycling lower continental crust in the north china craton. Nature, 432(7019), 892-7.

Gao, X.Y., Zhao, T.P., Bao, Z.W., Yang, A.Y., 2014a. Petrogenesis of the early Cretaceous intermediate and felsic intrusions at the southern margin of the North China Craton: implications for crust-mantle interaction. Lithos, 206, 65–78.

Griffin, W. L., Zhang, A., O'Reilly, S. Y., Ryan, C. G., 1998. Phanerozoic Evolution of the Lithosphere Beneath the Sino- Korean Craton. Mantle Dynamics and Plate Interactions in East Asia. American Geophysical Union (AGU).

Guo, P., Niu, Y., Ye, L., Liu, J., Sun, P., Cui, H., Zhang, Y., Gao, J., Su, L., Zhao, J., Feng, Y., 2014. Lithosphere thinning beneath west north china craton: evidence from geochemical and Sr–Nd–Hf isotope compositions of Jining basalts. Lithos, 202-203(4), 37-54.

Haase, K. M., Worthington, T. J., Stoffers, P., Garbe-Schönberg, D., Wright, I., 2002.

Mantle dynamics, element recycling, and magma genesis beneath the Kermadec arc-Havre trough. Geochemistry Geophysics Geosystems, 3(11), 1-22.

Hacker, B. R., Wang, X., Eide, E. A., Ratschbacher L., 1996. The Qinling–Dabie ultramafic-pressure collisional orogen. In The Evolution of Asia (eds. A. Yin and T. M. Harrison). Cambridge University Press, Cambridge, pp. 345-370.

Hickey-Vargas, R., Sun, M., Holbik, S., 2016. Geochemistry of basalts from small eruptive centers near villarrica stratovolcano, chile: evidence for lithospheric mantle components in continental arc magmas. Geochimica Et Cosmochimica Acta, 185, 358-382.

Holm, P. M., Søager, N., Alfastsen, M., Bertotto, G. W., 2016. Subduction zone mantle enrichment by fluids and Zr–Hf-depleted crustal melts as indicated by backarc basalts of the southern volcanic zone, argentina. Lithos, 262, 135-152.

Hilton, D. R., Hammerschmidt, K., Teufel, S., Friedrichsen, H., 1993. Helium isotope characteristics of andean geothermal fluids and lavas. Earth Planetary Science Letters, 120(3–4), 265-282.

Hoang, N., Uto, K., 2006. Upper mantle isotopic components beneath the Ryukyu arc system: evidence for ‘back-arc’ entrapment of pacific morb mantle. Earth Planetary Science Letters, 249(3–4), 229-240.

Hickey-Vargas, R., 1998. Origin of the Indian ocean- type isotopic signature in basalts from Philippine sea plate spreading centers: an assessment of local versus large- scale processes. Journal of Geophysical Research Solid Earth, 103(B9), 20963-20979.

Hsü, K.J., Wang, Q., Li, J., Zhou, D., Sun, S., 1987. Tectonic evolution of Qinling Mountains, China. Eclogae Geologicae Helvetiae, 80, 735-752.

Ishizuka, O., Yuasa, M., Tamura, Y., Shukuno, H., Stern, R. J., Naka, J., Joshima, M., Taylor, R.N., 2015. Migrating shoshonitic magmatism tracks Izu–Bonin–Mariana intra-oceanic arc rift propagation. Earth Planetary Science Letters, 294(1), 111-122.

Ishizuka, O., Taylor, R. N., Geshi, N., Oikawa, T., Kawanabe, Y., Ogitsu, I., 2015. Progressive mixed-magma recharging of izu-oshima volcano, japan: a guide to magma chamber volume. Earth Planetary Science Letters, 430, 19-29.

Ishizuka, O., Taylor, R. N., Yuasa, M., Ohara, Y., 2011. Making and breaking an Island arc: a new perspective from the Oligocene Kyushu-Palau arc. AGU Fall Meeting (Vol.135, pp.627615-627615-8). AGU Fall Meeting Abstracts.

Ishizuka, O., Geshi, N., Kawanabe, Y., Ogitsu, I., Taylor, R. N., Tuzino, T., 2014. Long-distance magma transport from arc volcanoes inferred from the submarine eruptive fissures offshore izu-oshima volcano, izu–bonin arc. Journal of Volcanology Geothermal Research, 285, 1-17.

Jahn, B.M., Auvray, B., Comichet, J., Bai, Y.L., Shen, Q.H., Liu, D.Y., 1987. 3.5 Ga old amphibolites from eastern Hebei province, China: field occurrence, petrography, Sm–Nd isochron age and REE geochemistry. Precambrian Research, 34, 31l–346l.

Jahn, B.M., Wu, F.Y., Chen, B., 2000a. Granitoids of the Central Asian orogenic belt and continental growth in the Phanerozoic. Transactions of the Royal Society of

Edinburgh, Earth Science, 91, 181–193.

Jahn, B.M., Wu, F.Y., Chen, B., 2000b. Massive granitoid generation in Central Asia: Nd isotope evidence and implication for continental growth in the Phanerozoic. Episodes, 23 (2), 82–92.

Jahn, B.M., Capdevila, R., Liu, D.Y., Vernon, A., Badarch, G., 2004. Sources of Phanerozoic granitoids in the transect Bayanhongor–Ulaan Baatar, Mongolia: geochemical and Nd isotopic evidence, and implications for Phanerozoic crustal growth. Journal of Asian Earth Sciences, 23 (5), 629-653.

Karason, H., van der Hilst R., 2000. Constraints on mantle convection from seismic tomography. Geophys Monogr, 121, 277–288.

Kong, J.J., Niu, Y.L., Duan, M., Zhang, Y., Hu, Y., Li, J.Y., Chen, S., 2017. Petrogenesis of Luchuba and Wachabab granitoids in western Qinling: Geochronology and geochemical evidence. Mineralogy and Petrology, 111, 887-908.

Kramer, W., Siebel, W., Romer, R. L., Haase, G., Zimmer, M., Ehrlichmann, R., 2005. Geochemical and isotopic characteristics and evolution of the jurassic volcanic arc between arica (18°30′s) and tocopilla (22°s), north chilean coastal cordillera. Chemie der Erde - Geochemistry, 65(1), 47-78.

Li, S. G., Chen Y., Cong B. L., Zhang Z., Zhang R., Liou, D., Hart S. R. Ge N., 1993. Collision of the North China and Yangtze blocks and formation of coesite-bearing eclogites: timing and processes. Chem Geol, 109, 70–89.

Li, X.H., 2000. Cretaceous magmatism and lithosphere extension in Southeast China.

Journal of Asian Earth Sciences, 18, 293–305.

Li, X.H., Li, W.X., Li, Z.X., Lo, C.H., Wang, J., Ye, M.F., Yang, Y.H., 2009. Amalgamation between the Yangtze and Cathaysia blocks in South China: constraints from SHRIMP U-Pb zircon ages, geochemistry and Nd-Hf isotopes of the Shuangxiwu volcanic rocks. Precambrian Research, 174, 117–128.

Li, Z., Qiu, J. S., Yang, X. M., 2014. A review of the geochronology and geochemistry of Late Yanshanian (Cretaceous) plutons along the Fujian coastal area of southeastern china: implications for magma evolution related to slab break-off and rollback in the cretaceous. Earth-Science Reviews, 128(1), 232-248.

Li, N., Chen, Y. J., Santosh, M., Pirajno, F., 2018. Late Mesozoic granitoids in the Qinling orogen, central china, and tectonic significance. Earth-Science Reviews, 182.

Li, S., Wang, T., Wilde, S. A., Tong, Y., 2013. Evolution, source and tectonic significance of early Mesozoic granitoid magmatism in the central Asian orogenic belt (central segment). Earth-science reviews, 126(11), 206-234.

Liu, D.Y., Nutman, A.P., Compston, W., Wu, J., She, Q., 1992. Remnants of N3800 Ma crust in the Chinese part of the Sino-Korean Craton. Geology, 20, 339–342.

Liu, Y., Gao, S., Yuan, H., Zhou, L., Liu, X., Wang, X.,Hu, Z., Wang, L., 2004. U–pb zircon ages and Nd, Sr, and Pb isotopes of lower crustal xenoliths from north china craton: insights on evolution of lower continental crust. Chemical Geology, 211(1), 87-109.

Liu, D. Y., Jian, P., Kro¨ner, A. Xu, S. T., 2006. Dating of prograde metamorphic

events deciphered from episodic zircon growth in rocks of the Dabie-Sulu UHP complex, China. Earth Planetary Science Letters, 250, 650–666.

Ma, C., Ehlers, C., Xu, C., Li, Z., Yang, K., 2000. The roots of the dabieshan ultrahigh-pressure metamorphic terrane: constraints from geochemistry and Nd–Sr isotope systematics. Precambrian Research, 102(3), 279-301.

Mamani, M., Worner, G., Sempere, T., 2010. Geochemical variations in igneous rocks of the central andean orocline (13 s to 18 s): tracing crustal thickening and magma generation through time and space. Geological Society of America Bulletin, 122(1), 162-182.

Mattauer, M., Matte, P., Malavielle, J., Tapponnier, P., Maluski, H., Xu, Z.Q., Lu, Y.L., Tang, Y.Q., 1985. Tectonics of Qinling belt: build-up and evolution of western Asia. Nature, 317, 496–500.

Menzies, M.A., Fan, W.M., Zhang, M., 1993. Paleozoic and Cenozoic lithoprobe and the loss of 120 km of Archean lithosphere, Sino-Korean Craton, China. Geol Soc Spec Publ, 76, 71–78.

Marske, J. P., Pietruszka, A. J., Trusdell, F. A., Garcia, M. O., 2011. Geochemistry of southern pagan island lavas, mariana arc: the role of subduction zone processes. Contributions to Mineralogy Petrology, 162(2), 231-252.

Mukasa, S. B., Mccabe, R., Gill, J. B., 2016. Pb-isotopic compositions of volcanic rocks in the west and east philippine island arcs: presence of the dupal isotopic anomaly. Earth Planetary Science Letters, 84(2), 153-164.

Niu, Y. L., 2009, Some basic concepts and problems on the petrogenesis of intra-plate

ocean island basalts. Chinese Sci Bull, 54, 4148-4160.

Niu, Y., 2005. Generation and evolution of basaltic magmas: Some basic concepts and a new view on the origin of Mesozoic-Cenozoic basaltic volcanism in eastern China, Geological Journal of China Universities, 11, 9–46.

Niu, Y.L., 2006. Continental lithospheric thinning results from hydration weakening, not ‘‘delamination’’, and is a special consequence of plate tectonics, for ‘‘mantleplume.org’’. http://www.mantleplumes.org/Hydration.html.

Niu, Y.L., 2014. Subduction initiation, trench retreat and global tectonic consequences: the origin of backarc basins in the western Pacific and effect on eastern China geology since the Mesozoic. In: Zhai, M.G., Xiao, W.J. (Eds.), Plate Tectonics, Geological Events and Resources: NewAdvances in Geological Sciences. Science Press, Beijing (Pages 15 pp.).

Niu, Y., Liu, Y., Xue, Q., Shao, F., Chen, S., Duan, M., Guo, P., Gong, H., Hu, Y., Hu, Z., Kong, J., Li, J., Liu, J., Sun, P., Sun, W., Ye, L., Xiao, Y., Zhang, Y., 2015. Exotic origin of the Chinese continental shelf: new insights into the tectonic evolution of the western Pacific and eastern China since the Mesozoic. Science Bulletin, 60(18), 1598-1616.

Olov, Nyström., Jan, Vergara., Mario, Morata., Diego, Levi, Beatriz., 2003. Tertiary volcanism during extension in the andean foothills of central chile (33°15'-33°45's). Geological Society of America Bulletin, 115(12), 1523-1537.

Okay, A. I., Sengo, r A. M. C., 1993. Tectonic of an ultra-highpressure metamorphic terrane: the Dabie Shan/Tongbai Shan orogen, China. Tectonics, 12, 1320–1334.

Parada, M. A., Rivano, S., Sepulveda, P., Herve, M., Herve, F., Puig, A., 1988. Mesozoic and cenozoic plutonic development in the andes of central chile (30°30′–32°30′s). Journal of South American Earth Sciences, 1(3), 249-260.

Pearce, J. A., Ernewein, M., Bloomer, S. H., Parson, L. M., Murton, B. J., Johnson, L. E., 1994. Geochemistry of lau basin volcanic rocks: influence of ridge segmentation and arc proximity. Geological Society London Special Publications, 81(1), 53-75.

Reagan, M. K., Ishizuka, O., Stern, R. J., Kelley, K. A., Ohara, Y., Blichert- Toft, J., 2013. Fore- arc basalts and subduction initiation in the izu- bonin- mariana system. Geochemistry Geophysics Geosystems, 11(3), 427-428.

Rudnick, R., Gao, S., 2003. Composition of the continental crust. Treatise on Geochemistry, 3, 1-64.

Savov, I. P., Hickeyvargas, R., D'Antonio, M., Ryan, J. G., Spadea, P., 2005. Petrology and geochemistry of west philippine basin basalts and early palau–kyushu arc volcanic clasts from odp leg 195, site 1201d: implications for the early history of the izu–bonin–mariana arc. Journal of Petrology, 47(2), 277-299.

Sengör, A.M.C., 1985. East Asian tectonic collage. Nature, 318, 16–17.

Smith, I. E. M., Worthington, T. J., Price, R. C., Stewart, R. B., Maas, R., 2006. Petrogenesis of dacite in an oceanic subduction environment: raoul island, kermadec arc. Journal of Volcanology Geothermal Research, 156(3), 252-265.

Smith, I. E. M., Price, R. C., Stewart, R. B., Worthington, T. J., 2009. An assessment of the mantle and slab components in the magmas of an oceanic arc volcano:

raoul volcano, kermadec arc. Journal of Volcanology Geothermal Research, 184(3), 437-450.

Soager, N., Holm, P. M., Llambías, E. J., 2013. Payenia volcanic province, southern mendoza, argentina: oib mantle upwelling in a backarc environment. Chemical Geology, 349-350(4), 36-53.

Stern, R. J., Kohut, E., Bloomer, S. H., Leybourne, M., Fouch, M., Vervoort, J., 2006. Subduction factory processes beneath the guguan cross-chain, mariana arc: no role for sediments, are serpentinites important? Contributions to Mineralogy Petrology, 151(2), 202-221.

Stern, R. J., Lin, P. N., Morris, J. D., Jackson, M. C., Fryer, P., Bloomer, S. H., 1990. Enriched back-arc basin basalts from the northern mariana trough: implications for the magmatic evolution of back-arc basins. Earth Planetary Science Letters, 100(1), 210-225.

Sun, P., Niu, Y.L., Guo, P.Y., Ye, L., Liu, J.J., Feng, Y.X., 2017. Elemental and Sr-Nd-Pb isotope geochemistry of the Cenozoic basalts in Southeast China: Insights into their mantle sources and melting processes. Lithos, 272-273, 16-30.

Sun, S-S., McDonough, W.F., 1989. Chemical and isotopic systematics of oceanic basalts: implications for mantle composition and processes. Geological Society, London, Special Publications, 42, 313–345.

Tamura, Y., Ishizuka, O., Stern, R. J., Nichols, A. R. L., Kawabata, H., Hirahara, Y.l., 2014. Mission immiscible: distinct subduction components generate two primary magmas at pagan volcano, mariana arc. Journal of Petrology, 55(1), 63-101.

Taylor, B., Natland, J., 2013. Coexistence of Indian and Pacific Oceanic Upper Mantle Reservoirs Beneath the Central New Hebrides Island Arc. Active Margins and Marginal Basins of the Western Pacific. American Geophysical Union.

Turner, S., Hawkesworth, C., Rogers, N., Bartlett, J., Worthington, T., Hergt, J., 1997. 238 U - 230 Th disequilibria, magma petrogenesis, and flux rates beneath the depleted tonga-kermadec island arc. Geochimica Et Cosmochimica Acta, 61(22), 4855-4884.

Vervoort, J.D., Blichert-Toft, J., 1999. Evolution of the depleted mantle: Hf isotope evidence from juvenile rocks through time. Geochim Cosmochim Acta, 63, 533–556.

Vervoort, J.D., Plank, T., Prytulak, J., 2011. The Hf–Nd isotopic composition of marine sediments. Geochim Cosmochim Acta, 75, 5903–5926.

Wan, Y. S., Li, R. W., Wilde, S. A., Liu, D. Y., Chen, Z. Y., Yan, L. L., Song, T. R. Yin, X. Y., 2005. UHP dating metamorphism and exhumation of the Dabie Orogen, China: evidence from SHRIMP dating of zircon and monazite from a UHP granitic gneiss cobble from the Hefei basin. Geochim Cosmochim Acta, 69, 4333–4348.

Wang, Y., Zhang, A., Fan, W., Zhang, Y., Zhang, Y., 2013. Origin of paleosubduction-modified mantle for silurian gabbro in the cathaysia block: geochronological and geochemical evidence. Lithos, 160-161(1), 37-54.

Wang, X., Wang, T., Zhang, C., 2013. Neoproterozoic, paleozoic, and mesozoic

granitoid magmatism in the qinling orogen, china: constraints on orogenic process. Journal of Asian Earth Sciences, 72(4), 129-151.

White, W.M., Albarède, F., Télouk, P., 2000. High-precision analysis of Pb isotope ratios by multi-collector ICP-MS. Chemical Geology, 167, 257–270.

Wiedenbeck, M, Alle. P., Corfu, F., Griffin,W.L., Meier,M., Oberli, F., Quadt, A., Roddick, J.C., Spiegel, W., 1995. Three natural zircon standards for U −Th−Pb, Lu−Hf, trace element and REE analyses. Geostand Newslett, 19, 1–23.

Windley, B.F., Alexeiev, D., Xiao, W., Kröner, A., Badarch, G., 2007. Tectonic models for accretion of the Central Asian Orogenic Belt. Journal of the Geological Society of London, 164, 31–47.

Workman, R.K., Hart, S.R., 2005. Major and trace element composition of the depleted MORB mantle (DMM). Earth Planetary Science Letters, 231, 53–72.

Wu, F.Y., Lin, J.Q., Wilde, S.A., Sun, D.Y., Yang, J.H., 2005a. Nature and significance of the Early Cretaceous giant igneous event in eastern China. Earth Planetary Science Letters, 233, 103–119.

Wu, F.Y., Yang, J.H., Wilde, S.A., Zhang, X.O., 2005b. Geochronology, petrogenesis and tectonic implications of the Jurassic granites in the Liaodong Peninsula, NE China. Chemical Geology, 221, 127–156.

Wu, F.Y., Ji, W. Q., Sun, D. H., Yang, Y. H., Li, X. H., 2012. Zircon U–Pb geochronology and Hf isotopic compositions of the Mesozoic granites in southern Anhui province, china. Lithos, 150(5), 6-25.

Xu, J., Zhang, B., Han, Y., 1997. Discovery of high radiogenic pb isotopic

composition from proterozoic mafic rocks in north qinling area and its implication. Chinese Science Bulletin, 42(1), 51-54.

Xu, Y.-G., 2001. Thermo-tectonic destruction of the Archean lithospheric keel beneath the Sino-Korean Craton in China: Evidence, timing and mechanism, Phys Chem Earth (A), 26, 747-757.

Yokoyama, T., Kobayashi, K., Kuritani, T., Nakamura, E., 2003. Mantle metasomatism and rapid ascent of slab components beneath island arcs: evidence from 238 u- 230 th- 226 ra disequilibria of miyakejima volcano, izu arc, japan. Journal of Geophysical Research Solid Earth, 108(B7).

Zhao, G.C., Wilde, S.A., Cawood, P.A., Sun, M., 2001. Archean blocks and their boundaries in the North China Craton: lithological, geochemical, structural and P–T path constraints and tectonic evolution. Precambrian Research, 107, 45–73.

Zhang, Y.R., 1985. The ancient Tongbai-Xinyang ophiolite zone and mélange. Regional Geology of China, 13, 143–158.

Zhang, G. W., Meng, Q. R., Yu, Z. P., Sun, Y., Zhou, D. W. Guo A. L., 1996. Orogenic processes and dynamics of the Qinling. Sci. China (Ser. D), 39, 225–234.

Zhang, H.F, Zhang, B.R, Zhao, Z.D, Luo, T.C., 1996. Continental crust subduction and collision along shangdan tectonic belt of east qinling, china-evidence from pb, nd and sr isotopes of granitoids. Science China Earth Sciences, 39(3), 273-282.

Zhang, H.F., Sun, M., Zhou, X.H., Fan, W.M., Zhai, M.G., Yin, J.F., 2002. Mesozoic lithosphere destruction beneath the North China Craton: evidence from major-,

traceelement and Sr-Nd-Pb isotope studies of Fangcheng basalts. Contrib Mineral Petrol, 144, 241–254.

Zhang, H.-F., SUN, M., Zhou, X.H., Zhou, M. F., Fan, W.M. Zheng J. P. 2003. Secular evolution of the lithosphere beneath the eastern North China Craton: evidence from Mesozoic basalts and high-Mg andesites. Geochimica et Cosmochimica Acta, 67 (22) , 4373-4387.

Zhang, H.-F., Ying, J.F., Xu, P., Ma, Y.G., 2004. Mantle olivine xenocrysts entrained in Mesozoic basalts from the North China craton: Implication for replacement process of lithospheric mantle. Chinese Sci Bull, 49, 961-966.

Zhang, L.G., 1995. Block-geology of Eastern Asia Lithosphere-Isotope Geochemistry and Dynamics of Upper Mantle Basement and Granite (in Chinese), Beijing: Science Press, 15-350.

Zhao Z. F., Zheng Y. F., Gao T. S., Wu Y. B., Chen F. K., Wu, F. Y., 2006. Isotopic constraints on age and duration of fluid assisted high-pressure eclogite-facies recrystallization during exhumation of deeply subducted continental crust in the Sulu orogen. J Metamorph Geol, 24, 687-702.

Zhao Z. F., Zheng Y. F., Wei C. S. Wu F. Y., 2007. Post collisional granitoids from the Dabie orogen in China: zircon U–Pb age, element and O isotope evidence for recycling of subducted continental crust. Lithos, 93, 248-272.

Zhou, X.-H., Sun, M., Zhang, G.-H., Chen, S.-H., 2002. Continental crust and lithospheric mantle interaction beneath North China: isotopic evidence from granulite xenoliths in Hannuoba, Sino-Korean craton. Lithos, 62, 111 - 124.

Zhou, X.M., Sun, T., Shen, W.Z., Shu, L.S., Niu, Y.L., 2006. Petrogenesis of Mesozoic granitoids and volcanic rocks in South China: a response to tectonic evolution. Episodes, 29, 26-33.

Zhu, R. X., Xu, Y.G., Zhu, G., Zhang, H. F., Xia, Q. K., Zheng, T. Y., 2013. Destruction of the north China Craton. Sci China Earth Sci, 55, 1565–1587.

Zhu, D. C., Zhao, Z. D., Niu, Y., Dilek, Y., Hou, Z. Q., Mo, X. X., 2013. The origin and pre-cenozoic evolution of the tibetan plateau. Gondwana Research, 23(4), 1429-1454.

## Figure captions:

**Fig. 1:** Simplified geological map of eastern continental China, showing the distribution of Jurassic-Cretaceous granitoids (after 1:1,000,000 Geological Map and Data Base by the Chinese Geological Survey, 2005). Our sampled plutons are distributed along a ~ 1300 km long traverse parallel to the inferred paleo-Pacific subduction from the southeast coastline to the Xiaoqinling in the continental interiors. Although, the exact paleo-Trench location is unknow, but is likely parallel to and in the vicinity of the South-East China coastal line indicated by thick gray dashed line (Niu et al., 2015). The thick gray-arrowed line indicates the shortest distance of each sampled pluton to the inferred continental arc (i.e., coastline of the southeast continental China). The tectonic units indicated are West Block (WB), East Block (EB) and Trans-North China Orogen (TNCO) of the North China Craton (NCC), Yangtze Craton (YZ) and Cathaysia Block (CB) of the South China Block and Qinling-Dabie

Orogen (QDO).

**Fig. 2:** Photomicrographs showing mineral assemblage of representative granitoids ((a) sample XX14-01, (b) sample WY14-07, (c) sample TTZ14-05, (d) sample CS14-01). The abbreviations are: Pl-plagioclase, Qz-quartz, Bt-biotite, Kfs-K-feldspar, Amp-amphibole.

**Fig. 3:** Zircon U-Pb Concordia diagrams of nine selected plutons represented by samples LN14-01, YL14-03, HC14-01, EDY14-01, HS14-02, CS14-01, BMJ14-01, LT14-03, LNS14-03. The crystallization ages for these plutons varies from 99.2 ± 2.0 to 146.7 ± 2.3 Ma with no obvious spatial correlation except for the youngest (~ 99.2 Ma) pluton represented by LN14-9 at the southeast cost (see Fig. 9 below).

**Fig. 4:** Total alkalis ($Na_2O$ + $K_2O$) versus $SiO_2$ (TAS) diagram showing the compositional variation of the plutons we study. They are mainly granitic in compositions.

**Fig. 5:** $SiO_2$ variation diagrams of representative major (wt. %) and selected trace (ppm) elements of the plutons/samples we study, showing large compositional variability with first-order trends consistent with varying extents of fractional crystallization although these plutons/samples do not share common liquid lines of descent in space and time.

**Fig. 6:** Primitive mantle-normalized (Sun and McDonouth, 1989) multi-element patterns for our studied plutons. The model bulk continental crust and lower continental crust (BCC and LCC; Rudnick and Gao, 2003) are plotted for comparison.

**Fig. 7:** Sr-Nd-Pb-Hf isotope co-variation diagrams of the plutons/samples we study.

The Sr-Nd-Pb isotopic compositions of the lower continental crust from the Dabie (DB), the North China Craton (NCC), the Northern Qinling (NQ), the south margin of the North China Craton (SMNCC), Yangzi Craton (YZ) and Cathaysia Block (CB) are plotted to compare (Chen and Jahn, 1998; Liu et al., 2004; Jahn et al., 1999; Ma et al., 2000; Zhang et al., 1995; Zheng et al., 2000; Xue et al., 2005; Zhang et al., 1996; Xu et al., 1997). The subcontinental lithospheric mantle is represented by the Mesozoic basalts in eastern continental China (Zhang et al., 2002, 2003; Guo et al., 2014). Sr, Nd, Pb and Hf isotopes for IAB are from west Pacific arcs (including Kermadec arc, Mariana arc, Izu-Bonin arc, Luzon arc, Ryukyu arc, Yap arc, Tonga arc, Andean arc, Smith et al., 2009; Smith et al., 2006; Ewart et al., 1977; Haase et al., 2002; Smith et al., 2010; Stem et al., 1990; Savov et al., 2005; Stern et al., 2006; Ishizuka et al., 2015; Ishizuka et al., 2011; Marske et al., 2011; Reagan et al., 2013; Tamura et al., 2014; Elliott et al., 1997; Ishizuka et al., 2014; Ishizuka et al., 2015; Yokoyama et al., 2003; Mukasa et al., 2016; Dufrane et al., 2006; Hoang and Uto, 2006; Shinjo et al., 2000; Hickey, 1998; Crawford et al., 1986; Beccaluva, 1980; Turner et al., 1997; Pearce et al., 1994; Taylor and Natland, 2013; Escrig et al., 2013; Béguelin et al., 2015; Chiaradia et al., 2014; Soager et al., 2013; Hickey-Vargas et al., 2016; Holm et al., 2016; Hilton et al., 1993; Vargas et al., 1989; Olov et al., 2003; Davidson and Silva, 1995; Kramer et al., 2005). Andean granites are from (Lucassen, 1999; Chiaradia, 2004; Chiaradia et al., 2004; Parada, 1988; Mamani et al., 2010). The NHRL (north hemisphere reference line) and DMM (Hart, 1984; Workman and Hart, 2005) are shown for comparison.

**Fig. 8:** Spatial variation of isotopic compositions, apparently showing that coastal granitoids (blue circles) are Nd (Hf) less enriched and Pb more enriched than interior granitoids (red circles). The interior granitoids show first-order spatial variation as a function of distance to the coastline of the southeast continental China, showing the location of the boundary of the coastal granitoids and the interior granitoids is ~400 km away from the southeastern coastline.

**Fig. 9:** Showing that the plutons/samples we study have no correlation in space and time. This supports the prediction that except for the coastline plutons, most of these inland plutons are not associated with the active subduction of the paleo-Pacific plate, but are genetically and ultimately associated with dehydration of the paleo-Pacific plate lying stagnantly in the mantle transition zone (Niu, 2014; Niu et al., 2015).

**Fig. 10:** Cartoon illustrating the concept of paleo-Pacific plate subduction-related coastal granitoids and subducted stagnant paleo-Pacific slab dehydration related widespread Jurassic-Cretaceous granitoids in the interior of continental China, with the latter involving re-working of mature lower continental crust.

## Table captions:

**Table 1:** Geological setting of studied plutons from the eastern China.

| Pluton | Location | Rock type | Description | References |
|---|---|---|---|---|
| Liangnong | Yuyao county Liangnong village | Granodiorite | The Liangnong intrusive complex is controled by NNE trending fault with composed of the Late Yanshanian granite and the Himalayan period granite. It crops out over an area of about 88.19 $km^2$, and intrudes Lower Cretaceous and Upper Jurassic strata. And it is overlain by Pliocene basalts of the Shengxian group. | Gao et al., 2014 |

| | | | | |
|---|---|---|---|---|
| Hecun | Southwest part of Yinzhubu area | Granite | This pluton intrudes Jurassic Yushanjian group and Wuzhao group, Ordovician strata of Yinzhubu group, Ningguo group, Hule group. | [1]; Wu et al., 2012 |
| Moganshan | Eastern Tianmu mountain Early Cretaceous volcanic basin | Mainly middle-coarse grained and locally fine grained biotite K-feldspar granite and biotite monzogranite | The Moganshan pluton is controlled by NE trending Yucun fault, and outcrops 9.8 $km^2$ in the term of small irregular-shaped rock. It intrusively touchs with rhyolitic and dacitic volcanic rocks of Jiande group Huangjian series. | Zhang et al., 2012 |
| Yunling | West part of Guanling area | Granodiorite | This pluton is distributed of NE trending, and overlian by the Quaternary strata, with formation of the Yunling golden mine. | Wu et al., 2012; Liu, 2014 |
| Tianzhushan | Near Wuhe-Shuihou fault (WSF) | Mainly fine grained granodiorite with locally middle-fine grained diorite and quartz monzonite | This pluton is located at Wuhe-Shuihou fault which delimits the South Dabie ultra-pressure metamorphic belt and the North Dabie complex with NW to SE irregular extension. It is composed of few intrusive units and outcrops area of 120$km^2$. | Peng et al., 1994 |
| Baimajian | Northwest part of the Eastern Dabie | Monzogranite and syenitegranite | The Baimajian pluton outcrops over 1000$km^2$ with few small intrusive unit of granodiorite and distribution of metamorphic rocks that are dominated by gneiss and eclogite. The contact between the granitic pluton and the Dabie complex in the region are generally sharp. | Zhang and Du, 1998; Kuang et al., 1999; Wang and Cong, 1998; Xue et al., 1994 |

| | | | | |
|---|---|---|---|---|
| Tiantangzhai | At the core of Dabie Mountain | Porphyritic granite | This pluton crops out over an area of 100km$^2$, intrusively contact with the Dabie gneiss and the early period pluton. | Sang et al., 2000; Deng, 2013 |
| Shangcheng | From parts of the SN trending Shangcheng-Macheng fault (SMF) and the EW trending Guishan-Meishan fault (GMF) | Porphyritic granodiorite and porphyritic monzogranite | This pluton intrudes Carboniferous detrital rocks of Yangxiaozhuang group, Upper Jurassic volcanic rocks of Jingangtai group, Lower Cretaceous volcanic rocks, Middle-Neo Proterozoic metamorphic rocks of Guishan groups and Late Jurassic quartz monzodiorite of Chenxiangpu group. And it outcrops 131km$^2$ area. | Liu et al., 2003 |
| Xinxian | In county of Chengguan village, Doushanhe village and Sidian village | Granite, porphyritic granite and quartz monzonite | This pluton outcrops an area of 190 km$^2$, with intrusive contacting with the host. And its south part intrudes Lower Proterozoic Xinxian group, middle part intrudes Lower Proterozoic Qijiaoshan group, north part intrudes Middle Proterozic Huwan group. The contact surface trends to the pluton. | Chen et al., 2013; Zhao et al., 2013 |
| Jigongshan | Outcroping in Jigongshan and Pingjingguan area | Monzogranite | This pluton intrudes Tongbai gneiss, and intruded by Cheyunshan pluton and Lingshan pluton. And it has NW trending belt distribution. | Wei et al., 2016 |
| Chunshui | North part of the North Qinling-North Huaiyang tectonic belt | Monzogranite, alkali feldspar granite and K-feldspar granite | This study area is divided into Huangshan, Zushiding and Jiaozishan three plutons from south to north. Huangshan pluton has NW-SE trending distribution and intrudes Neoproterozoic granite of Kuanping and Ruyang group. Zushiding pluton is located at the middle part of the study area with NW-SE distribution and intrusdes Ruyang group, being overlain by Quaternary strata. Jiaozishan pluton is located at the northest area. Its south part intrudes Neoproterozic granite and north part intrudes Ruyang group. | Zhou et al., 2008 |
| Erdaoya | East part of Nanzhao county | Granite | This pluton intrudes the Proterozoic Songshan group, Maoji group and Sujiahe group. | [2] |

| | | | | |
|---|---|---|---|---|
| Taishanmiao | North part of the EW trending Machaoying fault | Porphyritic granite, monzogranite and fine grained granite | This pluton outcrops an area of 300 $km^2$, with NE intruding the Middle Proterozoic strata of Xionger group Jidanping series. It belongs to Xionger-Waifangshan ore-formation areas of the North China margin ore-formation belt. | Ye et al., 2008; Ma et al., 2008 |
| Heyu | Located in the vicinity of Luanchuan county Heyu | Monzogranite and porphyritic granite | This pluton is the biggest granitic pluton in the Yuxi district with croping out over an area of 784 $km^2$. It is formed by four times magmatic intrusion, the first stage at the core, the second stage around the first stage, the third stage is the biggest that located at the margin of the complex, the fourth stage is Yanshanian granitoids. | Guo, 2009 |
| Huashan | Late period intrusion at the north margin of the Songping pluton | Granite | This pluton outcrops an area of 130$km^2$, with irregularly EW trending distribution. The host is Taihua group. | Meng et al., 2012 |
| Wenyu | Middle east part of the Xiaoqinling area | Monzogranite | This pluton outcrops an area of 71 $km^2$, with three phase belts. The margin phase is fine, middle-fine grained biotite monzogranite. Mainly part of the excessive phase is gray-white middle grained biotite monzogranite. The top phase is gray-white fine grained biotite monzogranite. | Wang et al., 2010 |
| Laoniushan | Located in a zone between the southern margin of NCC and the North Qinling belt, northwest of the Dabie ultra-high pressure (UHP) orogenic belt | Biotite monzogranite, quartz diorite, hornblende monzonite, and quartz monzonite | The Laoniushan intrusive complex is a lenticular body that crops out over an area of about 440 $km^2$. It intrudes various Precambrian metamorphic rocks, including the Archean Taihua Group gneiss, the Paleoproterozoic Tietonggou Group quartzite, the Xiong'er Group mafic volcanic rocks and quartzites, and the Gaoshanhe Group slates. | Ding et al., 2011; Qi et al., 2012 |
| Lantian | Southeast of the Lantian county | Monzogranite | This complex outcrops an area of 154 $km^2$, with EW trending distribution. Its south part intrudes the Tietonggou group, and east part intrudes the Taihua group. | Ding et al., 2010 |
| Note: [1-2] from 1:500,000 geological map of Zhejiang province and Henan province | | | | |

| | |
|---|---|
| (http://www.ngac.org.cn/Map) | |

**Table 2:** Petrography of studied plutons from the eastern China.

| Pluton | Sample | Longitude (°, N) | Latitude (°, E) | shortest distance to Arc (km) | Rock type | Petrograpic description | Age (Ma) | Age data source |
|---|---|---|---|---|---|---|---|---|
| Liangnong | LN14-09 | 29.85 | 121.09 | 116 | granitoids | Fresh; fine grained, K-feldspar granite, plagioclase (~ 32%), K-feldspar (~ 38%), quartz (~ 25%), amphibole and biotite (~ 5%); accessory minerals are zircon, magnetite, titanite and apatite. | 99.2 ± 2.0 | this study |
| Hecun | HC14-01 | 29.83 | 119.62 | 244 | quartz monzonite | Fresh; medium grained, flesh pink in color, monzogranite, plagioclase (~ 33%), K-feldspar (~ 38%), quartz (~ 24%), amphibole and biotite (~ 5%); accessory minerals are zircon, magnetite, titanite and apatite, contains small mafic | 136.1 ± 2.0 | this study |

| | | | | | | | | |
|---|---|---|---|---|---|---|---|---|
| | | | | | | xenoliths. | | |
| Mogans han | MGS1 4-02 | 30.62 | 119.90 | 260 | granite | Fresh; fine-to-medium grained, flesh pink in color, K-feldspar granite, plagioclase (~ 30%), K-feldspar (~ 42%), quartz (~ 23%), amphibole and biotite (~ 5%); accessory minerals are zircon, magnetite, titanite and apatite, contains small mafic xenoliths. | 128.1 ± 2.1 | Zhang et al., 2012 |
| Yunling | YL14-02 | 30.61 | 118.21 | 410 | granodiorite | Fresh; fine grained, pale-gray in color porphyric, plagioclase (~ 40%), K-feldspar (~15 %), quartz (~ 30%), amphibole and biotite (~ 15%); accessory minerals are zircon and apatite. | 138.7 ± 1.8 | this study |
| Tianzhu shan | TZS14-02 | 30.71 | 116.40 | 567 | granite | Fresh; medium-to-coarse grained, monzogranite, plagioclase (~ 36%), | 128 ± 3.0 | Niu et al., 2015 |

| | | | | | | | | |
|---|---|---|---|---|---|---|---|---|
| | | | | | | K-feldspar (~ 35%), quartz (~ 24%), amphibole and biotite (~ 5%); accessory minerals are zircon, magnetite, titanite and apatite. | | |
| Baimajian | BMJ14-01 | 31.14 | 116.33 | 591 | granite | Fresh; fine-to-medium grained, monzogranite, plagioclase (~ 33%), K-feldspar (~ 37%), quartz (~ 25%), amphibole and biotite (~ 5%); accessory minerals are zircon, magnetite, titanite and apatite. | 125.4 ± 2.8 | this study |
| Tiantangzhai | TTZ14-05 | 31.28 | 115.59 | 661 | syenite | Fresh; flesh pink in color, medium-to-coarse grained, K-feldspar granite, plagioclase (~ 10%), K-feldspar (~ 73%), quartz (~ 12%), amphibole and biotite (~ 5%); accessory minerals are zircon, | 131 ± 1.0 | Niu et al., 2015 |

| | | | | | | | | |
|---|---|---|---|---|---|---|---|---|
| | | | | | | magnetite, titanite and apatite. | | |
| Shangcheng | SC14-02 | 31.77 | 115.23 | 716 | granodiorite | Fresh; fine grained, porphyric, plagioclase (~ 45%), quartz (~ 40%), amphibole and biotite (~ 15%); accessory minerals are zircon, magnetite, titanite and apatite. | 137 ± 1.2 | Niu et al., 2015 |
| Xinxian | XX14-01 | 31.71 | 114.81 | 750 | granite | Fresh; flesh pink in color, medium-to-coarse grained, K-feldspar granite, plagioclase (~ 30%), K-feldspar (~ 42%), quartz (~ 23%), amphibole and biotite (~ 5%); accessory minerals are zircon, magnetite, titanite and apatite. | 123.6 ± 1.1 | Niu et al., 2015 |
| Jigongshan | JGS14-01 | 31.84 | 114.07 | 820 | granite | Fresh; flesh pink in color, fine-to-medium grained, K-feldspar granite, plagioclase (~ 30%), | 128 ± 1.2 | Wei et al., 2016 |

| | | | | | | | | |
|---|---|---|---|---|---|---|---|---|
| | | | | | | K-feldspar (~ 43%), quartz (~ 22%), amphibole and biotite (~ 5%); accessory minerals are zircon, magnetite, titanite and apatite. | | |
| Chunshui | CS14-01 | 33.03 | 113.42 | 924 | granite | Fresh; pale-gray in color, medium grained, biotite monzogranite, plagioclase (~ 50%), K-feldspar (~ 20%), quartz (~ 26%), amphibole and biotite (~ 4%); accessory minerals are zircon, titanite and apatite. | 133.4 ± 1.5 | this study |
| Erdaoya | EDY14-01 | 33.74 | 112.45 | 1033 | granite | Fresh; pale-gray in color medium-to-coarse grained, monzogranite, plagioclase (~ 34%), K-feldspar (~ 36%), quartz (~ 25%), amphibole and biotite (~ 6%); accessory minerals are zircon, magnetite, | 138.1 ± 2.4 | this study |

| | | | | | | | | |
|---|---|---|---|---|---|---|---|---|
| | | | | | | titanite and apatite. | | |
| Taishan miao | TSM14-02 | 33.79 | 112.25 | 1053 | granite | Minor alteration; medium-to-coarse grained, alkali feldspar granite, plagioclase (~ 30%), K-feldspar (~ 43%), quartz (~ 22%), amphibole and biotite (~ 5%); accessory minerals are zircon, magnetite, titanite and apatite. | 115 ± 1.0 | Niu et al., 2015 |
| Heyu | HY14-09 | 33.98 | 111.86 | 1094 | granodiorite | Fresh; fine-to-medium grained, porphyric, plagioclase (~ 35%), K-feldspar (~ 15%), quartz (~ 35%), amphibole and biotite (~ 15%); accessory minerals are zircon and apatite. | 134 ± 2.5 | Niu et al., 2015 |
| Huashan | HS14-02 | 34.32 | 111.71 | 1119 | granite | Fresh; coarse grained, biotite monzogranite, plagioclase (~ 33%), K-feldspar (~ 37%), quartz (~ 25%), | 132.5 ± 1.5 | this study |

| | | | | | | | | |
|---|---|---|---|---|---|---|---|---|
| | | | | | | amphibole and biotite (~ 5%); accessory minerals are zircon, magnetite, titanite and apatite. | | |
| Wenyu | WY14-07 | 34.51 | 110.48 | 1233 | granite | Fresh; pale-gray in color, fine-to-medium grained, biotite monzogranite, plagioclase (~ 42%), K-feldspar (~ 33%), quartz (~ 20%), amphibole and biotite (~ 5%); accessory minerals are zircon, magnetite, titanite and apatite. | 131±3.0 | Niu et al., 2015 |
| Laonius han | LNS14-03 | 34.38 | 110.00 | 1267 | granite | Fresh; flesh pink in color, medium-to-coarse grained, K-feldspar granite, plagioclase (~ 30%), K-feldspar (~ 43%), quartz (~ 22%), amphibole and biotite (~ 5%); accessory minerals are zircon, magnetite, | 143.4±2.3 | this study |

| | | | | | | | | |
|---|---|---|---|---|---|---|---|---|
| | | | | | | titanite and apatite. | | |
| Lantian | LT14-03 | 34.12 | 109.44 | 1310 | granite | Fresh; medium-to-coarse grained, biotite monzogranite, plagioclase (~ 33%), K-feldspar (~ 35%), quartz (~ 27%), amphibole and biotite (~ 5%); accessory minerals are zircon, magnetite, titanite and apatite. | 146.7± 2.3 | this study |

**Table 3:** Sr-Nd-Hf-Pb isotopic compositions of studied granitoids from the eastern China.

| Laboratory | Samples | $^{87}Sr/^{86}Sr$ | 2σ | $^{143}Nd/^{144}Nd$ | 2σ | $^{176}Hf/^{177}Hf$ | 2σ | $^{208}Pb/^{204}Pb$ | 2σ | $^{207}Pb/^{204}Pb$ | 2σ | $^{206}Pb/^{204}Pb$ | 2σ | $^{87}Sr/^{86}Sr(t)$ | $^{143}Nd/^{144}Nd(t)$ | $^{176}Hf/^{177}Hf(t)$ | $^{208}Pb/^{204}Pb(t)$ | $^{207}Pb/^{204}Pb(t)$ | $^{206}Pb/^{204}Pb(t)$ | $\varepsilon_{Nd}(t)$ | $\varepsilon_{Hf}(t)$ | Age (Ma) | Age data source |
|---|---|---|---|---|---|---|---|---|---|---|---|---|---|---|---|---|---|---|---|---|---|---|---|
| UQ | LN14-09 | 0.711019 | 7 | 0.512287 | 5 | 0.282607 | 5 | 39.00052 | 25 | 15.656567 | 7 | 18.514145 | 8 | 0.700800 04 | 0.512223 | 0.282594 | 38.7551 | 15.6488 | 18.3200 | -5.6 | -4.1 | 99.2 ± 2.0 | this study |
| | HC14-01 | 0.711253 | 9 | 0.512310 | 5 | 0.282607 | 5 | 38.70000 | 28 | 15.584 7 | 8 | 18.36 14 | 8 | 0.700804 8 | 0.512195 | 0.282562 | 38.3433 | 15.5570 | 18.0051 | -5.2 | -4.4 | 136.1 ± 2.0 | this study |
| | MGS14-02 | 0.754702 | 11 | 0.512298 | 5 | 0.282630 | 5 | 39.18388 | 34 | 15.622 3 | 9 | 18.9283 | 9 | 0.700815 1 | 0.512172 | 0.282563 | 38.5332 | 15.5591 | 18.2664 | -5.9 | -4.6 | 128.1 ± 2.1 | Zhang et al., 2012 |
| | YL14-02 | 0.709059 | 9 | 0.512098 | 4 | 0.282400 | 6 | 39.03669 | 35 | 15.623 6 | 10 | 18.7736 | 9 | 0.700779 2 | 0.512196 | 0.282369 | 38.4422 | 15.6033 | 18.3449 | -9.0 | -11.2 | 138.7 ± 1.8 | this study |

| | | | | | | | | | | | | | | | | | | | | | | |
|---|---|---|---|---|---|---|---|---|---|---|---|---|---|---|---|---|---|---|---|---|---|---|
| | TZS14-02 | 0.711234 | 10 | 0.5116008 | 5 | 0.2820004 | 5 | 37.50094 | 37 | 15.34146 | 10 | 16.48225 | 8 | 0.7007583 | 0.51153 0 | 0.2819888 | 37.1522 | 15.3334 | 16.3119 | -18.4 | -24.9 | 128±3.0 | Niu et al., 2015 |
| | BMJ14-01 | 0.712572 | 9 | 0.5112449 | 4 | 0.2818819 | 5 | 37.32228 | 31 | 15.22668 | 9 | 15.95514 | 7 | 0.7089799 | 0.5111 69 | 0.2818003 | 36.9888 | 15.221 | 15.8827 | -25.5 | -31.5 | 125.4±2.8 | this study |
| | TTZ14-05 | 0.710290 | 8 | 0.5116500 | 4 | 0.2821300 | 5 | 38.05531 | 31 | 15.42199 | 8 | 16.99244 | 7 | 0.7090306 | 0.5115 76 | 0.2821144 | 37.7199 | 15.4199 | 16.9299 | -17.4 | -20.4 | 131±1.0 | Niu et al., 2015 |
| | SC14-02 | 0.708937 | 8 | 0.5114887 | 4 | 0.2819355 | 5 | 37.49996 | 24 | 15.30399 | 7 | 16.46777 | 6 | 0.7079311 | 0.5114 01 | 0.2819228 | 37.3233 | 15.2932 | 16.2116 | -20.7 | -26.8 | 137±1.2 | Niu et al., 2015 |
| | XX14-01 | 0.735741 | 8 | 0.5115200 | 5 | 0.2820092 | 5 | 37.79044 | 29 | 15.33773 | 9 | 16.80009 | 8 | 0.7079211 | 0.5114 46 | 0.2820078 | 37.4544 | 15.3288 | 16.6122 | -20.2 | -21.8 | 123.6±1.1 | Niu et al., 2015 |
| | JGS14 | 0.70 | 8 | 0.511 | 5 | 0.281 | 5 | 37.54 | 30 | 15.30 | 9 | 16.663 | 8 | 0.707 | 0.5114 50 | 0.281 | 37.38 | 15.30 | 16.500 | -20.0 | -26.9 | 128±1. | Wei et al., |

| | | | | | | | | | | | | | | | | | | | | | | |
|---|---|---|---|---|---|---|---|---|---|---|---|---|---|---|---|---|---|---|---|---|---|---|
| | -01 | 88088 | | 538 | | 939 | | 38 | | 89 | | 13 | | 784 | | 931 | 6 | 3 | 8 | | | 2 | 2016 |
| | CS14-01 | 0.7107021 | 11 | 0.5111885 | 5 | 0.2822274 | 5 | 38.11170 | 32 | 15.46229 | 9 | 17.36558 | 8 | 0.7084459 | 0.51180 2 | 0.2822633 | 37.7796 | 15.4544 | 17.177 | -13.0 | -15.1 | 133.4 ± 1.5 | this study |
| | EDY14-01 | 0.7097488 | 8 | 0.5111752 | 5 | 0.2821888 | 4 | 37.91997 | 30 | 15.45574 | 9 | 17.17722 | 8 | 0.7087225 | 0.51 1669 | 0.2821800 | 37.8422 | 15.4555 | 17.1130 | -15.5 | -17.9 | 138.1 ± 2.4 | this study |
| | TSM14-02 | 0.7145332 | 9 | 0.5111893 | 5 | 0.2823500 | 4 | 38.73776 | 31 | 15.48337 | 8 | 17.66661 | 8 | 0.7090700 | 0.51 1814 | 0.2823200 | 38.1118 | 15.4722 | 17.3449 | -13.2 | -22.2 | 115 ± 1.0 | Niu et al., 2015 |
| | HY14-09 | 0.7117000 | 8 | 0.5111728 | 5 | 0.2822228 | 5 | 38.81669 | 28 | 15.55132 | 8 | 17.79855 | 7 | 0.7091000 | 0.51 1650 | 0.2822119 | 38.3255 | 15.5033 | 17.6222 | -15.9 | -16.1 | 134 ± 2.5 | Niu et al., 2015 |
| | HS14-02 | 0.7094944 | 10 | 0.5111712 | 5 | 0.2822079 | 5 | 38.04355 | 30 | 15.47266 | 9 | 17.44477 | 8 | 0.7082366 | 0.51 1632 | 0.2820622 | 37.8777 | 15.4688 | 17.4544 | -16.3 | -18.3 | 132.5 ± 1.5 | this study |

| | | | | | | | | | | | | | | | | | | | | | | |
|---|---|---|---|---|---|---|---|---|---|---|---|---|---|---|---|---|---|---|---|---|---|---|
| | WY14-07 | 0.709356 | 9 | 0.511845 | 5 | 0.282252 | 6 | 38.37551 | 29 | 15.50200 | 8 | 17.80067 | 8 | 0.708444 | 0.5117759 | 0.282237 | 38.1887 | 15.4933 | 17.4233 | -13.9 | -13.5 | 131±3.0 | Niu et al., 2015 |
| | LNS14-03 | 0.711062 | 9 | 0.511737 | 6 | 0.282183 | 5 | 38.11131 | 30 | 15.54929 | 8 | 17.76271 | 7 | 0.708628 | 0.5116644 | 0.282165 | 37.9335 | 15.4885 | 17.5887 | -15.8 | -16.6 | 143.4±2.3 | this study |
| | LT14-03 | 0.711195 | 7 | 0.511984 | 6 | 0.282372 | 5 | 38.35117 | 37 | 15.50051 | 10 | 17.77105 | 9 | 0.708227 | 0.5118889 | 0.282361 | 37.9700 | 15.4911 | 17.4211 | -10.9 | -11.3 | 146.7±2.3 | this study |
| IOCAS | LN14-09REP | 0.711026 | 8 | 0.512275 | 3 | 0.282618 | 7 | 38.97900 | 18 | 15.65668 | 6 | 18.50455 | 6 | 0.708010 | 0.5122211 | 0.282605 | 38.6944 | 15.6466 | 18.3100 | -5.6 | -4.1 | 99.2±2.0 | this study |
| | MGS14-02REP | 0.754990 | 10 | 0.512261 | 4 | 0.282628 | 4 | 39.03334 | 24 | 15.62100 | 9 | 18.89411 | 11 | 0.708438 | 0.5121235 | 0.282560 | 38.3044 | 15.5585 | 18.2300 | -5.9 | -4.6 | 128.1±2.1 | Zhang et al., 2012 |
| | BMJ14- | 0.71 | 9 | 0.511 | 4 | 0.281 | 10 | 37.288 | 23 | 15.22 | 9 | 15.94 | 8 | 0.708 | 0.5111127 | 0.281 | 36.90 | 15.22 | 15.81 | -25.5 | -31.5 | 125.4± | this study |

| | | | | | | | | | | | | | | | | | | | | | | | |
|---|---|---|---|---|---|---|---|---|---|---|---|---|---|---|---|---|---|---|---|---|---|---|---|
| | 01REP | 2573 | | 208 | | 843 | | 26 | | 73 | | 35 | | 980 | | 826 | 8 | 1 | 9 | | | 2.8 | |
| | SC14-02REP | 0.708939 | 8 | 0.511457 | 4 | 0.281938 | 7 | 37.49800 | 19 | 15.31225 | 6 | 16.50229 | 6 | 0.707932 | 0.51 13 71 | 0.281931 | 37.3000 | 15.2995 | 16.2552 | -20.7 | -26.8 | 137 ± 1.2 | Niu et al., 2015 |
| | LNS14-03REP | 0.711035 | 6 | 0.511722 | 3 | 0.282189 | 5 | 38.11104 | 21 | 15.50225 | 7 | 17.63778 | 8 | 0.708601 | 0.51 16 29 | 0.282171 | 37.9100 | 15.4933 | 17.4655 | -15.8 | -16.6 | 143.4± 2.3 | this study |

REP: replicate sample. UQ represents samples analysed at the Radiogenic Isotope Facility at The University of Queensland, Australia; IOCAS represents samples reanalysed at the Laboratory of Ocean Lithosphere and Mantle Dynamics (IOCAS), Institute of Oceanology, Chinese Academy of Sciences. Age data were used to calculate the initially isotopic data.

$(^{87}Sr/^{86}Sr)_{(t)} = (^{87}Sr/^{86}Sr)_{Sample} - {}^{87}Rb/^{86}Sr(e^{\lambda t} - 1)$, $\lambda = 1.42 \times 10^{-11} a^{-1}$, t = Age Ma.

$(^{143}Nd/^{144}Nd)_t = (^{143}Nd/^{144}Nd) - (^{147}Sm/^{144}Nd) \times (e^{\lambda t} - 1)$, $\varepsilon_{Nd}(t) = [(^{143}Nd/^{144}Nd) / (^{143}Nd/^{144}Nd)_{CHUR}(t) - 1] \times 10^4$, $(^{143}Nd/^{144}Nd)_{CHUR}(t) = 0.512638 - 0.1967 \times (e^{\lambda t} - 1)$, $\lambda_{Sm\text{-}Nd} = 6.54 \times 10^{-12} a^{-1}$, t = Age Ma.

$(^{176}Hf/^{177}Hf)_t = [(^{176}Hf/^{177}Hf) - (^{176}Lu/^{177}Hf) \times (e^{\lambda t} - 1)$, $\varepsilon_{Hf}(t) = [(^{176}Hf/^{177}Hf) / (^{176}Hf/^{177}Hf)_{CHUR}(t) - 1] \times 10^4$, $(^{176}Lu/^{177}Hf)_{CHUR} = 0.0332$, $^{176}Hf/^{177}Hf_{CHUR} = 0.282772$, $\lambda = 1.867 \times 10^{-11} a^{-1}$, t = Age Ma.

Initial Pb isotope ratios were calculated by t = Age Ma. $(^{207}Pb/^{204}Pb)_{NHRL} = 0.1084 \times (^{206}Pb/^{204}Pb)_t + 13.491$, $(^{208}Pb/^{204}Pb)_{NHRL} = 1.209 \times (^{206}Pb/^{204}Pb)_t + 15.627$ (Hart, 1984).

## Appendixes

**Appendix A:** Major and trace element abundances of representative samples from the eastern China.

**Appendix B:** Bulk-rock major elements analyses at the IOCAS for the USGS reference material STM-2, RGM-2 and W-2.

**Appendix C:** Bulk-rock trace elements analyses at the IOCAS for the USGS reference material BCR-2, BHVO-2, AGV-2, RGM-2 and GSP-2.

**Appendix D:** Sr-Nd-Pb-Hf isotope analyses at the UQ and IOCAS for the USGS reference material BCR-2, JG-3, AGV-2 and GSP-2.

**Appendix E:** LA-ICP-MS UPb zircon data of nine studied samples.

**Appendix F:** Figures illustrate that five samples (LN14-09, MGS14-02, BMJ14-01, SC14-02, LNS14-03) reanalyze at the IOCAS, and the Sr-Nd-Pb-Hf isotope data obtained from UQ are fully reproducible.

**Appendix G:** Figures illustrate that there is no systematic isotopes variation as a function of ages.

**Appendix H:** Figure illustrate that the age difference of interior granitoids have nothing to do with their spatial differences in the Qinling-Dabie Orogenic belt.

Highlights:

- The interior granitoids have different sources and petrogenesis than coastal granitoids.
- The interior granitoids result from basal hydration weakening induced crustal melting.
- The coastal granitoids result directly from the paleo-Pacific plate subduction.

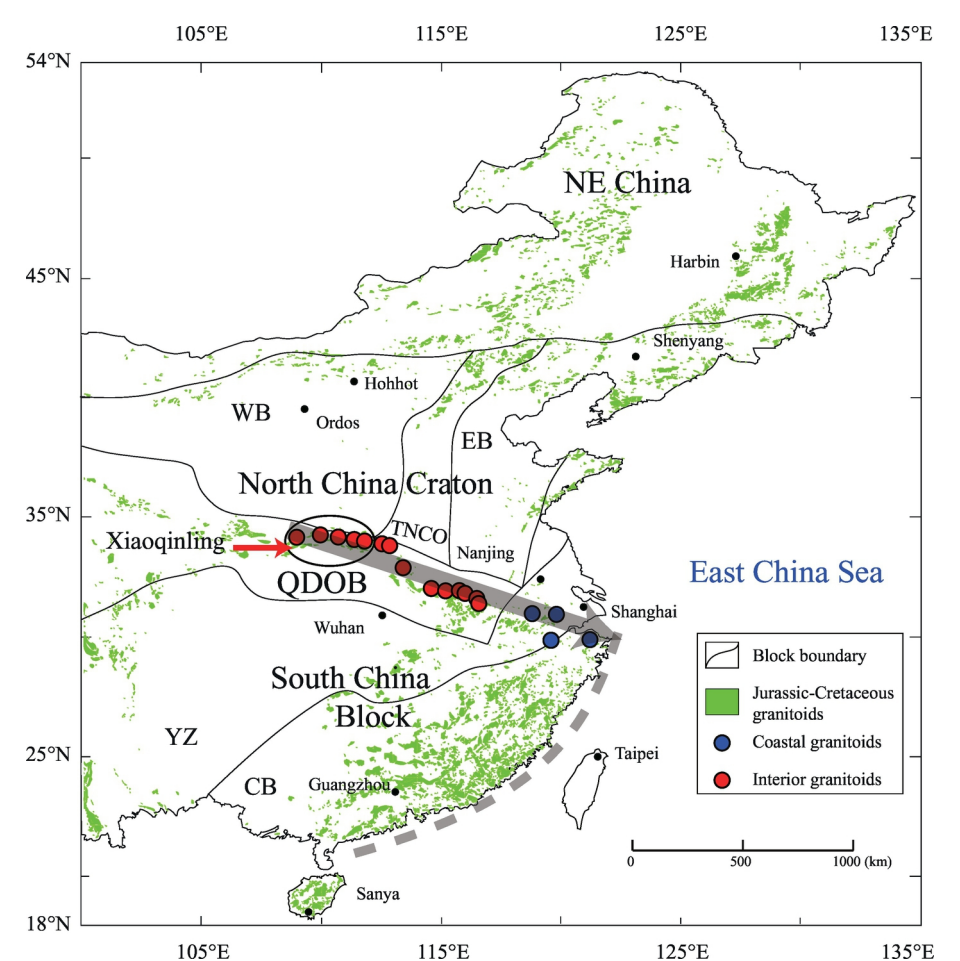
105°E
115°E
125°E
135°E
54°N
45°N
35°N
25°N
18°N
NE China
Harbin
Shenyang
Hohhot
WB
Ordos
EB
North China Craton
TNCO
Xiaoqinling
QDOB
Nanjing
East China Sea
Shanghai
Wuhan
South China
Block
YZ
CB
Guangzhou
Taipei
Sanya
Block boundary
Jurassic-Cretaceous granitoids
Coastal granitoids
Interior granitoids
0
500
1000 (km)

Figure 1

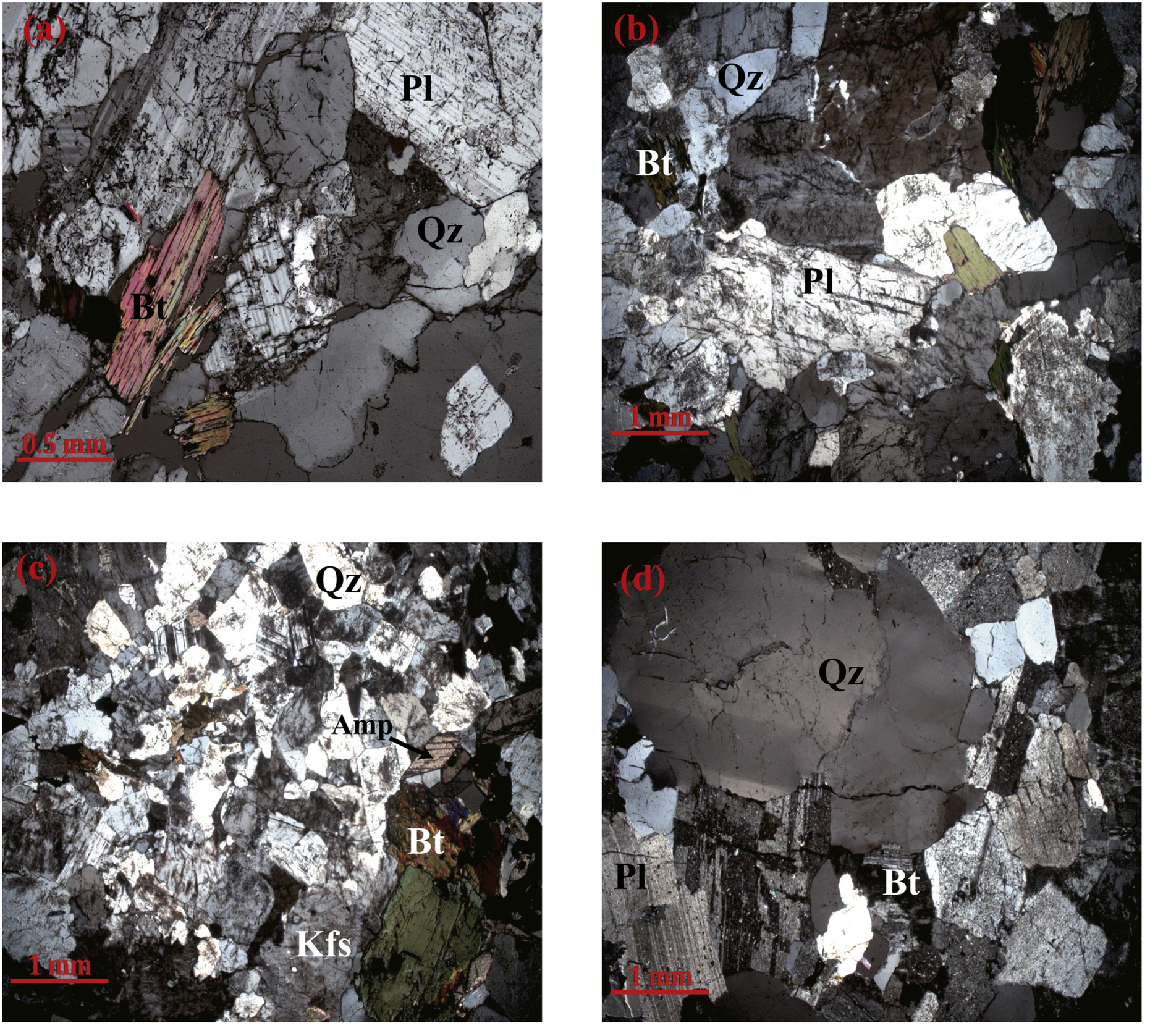


Figure 2

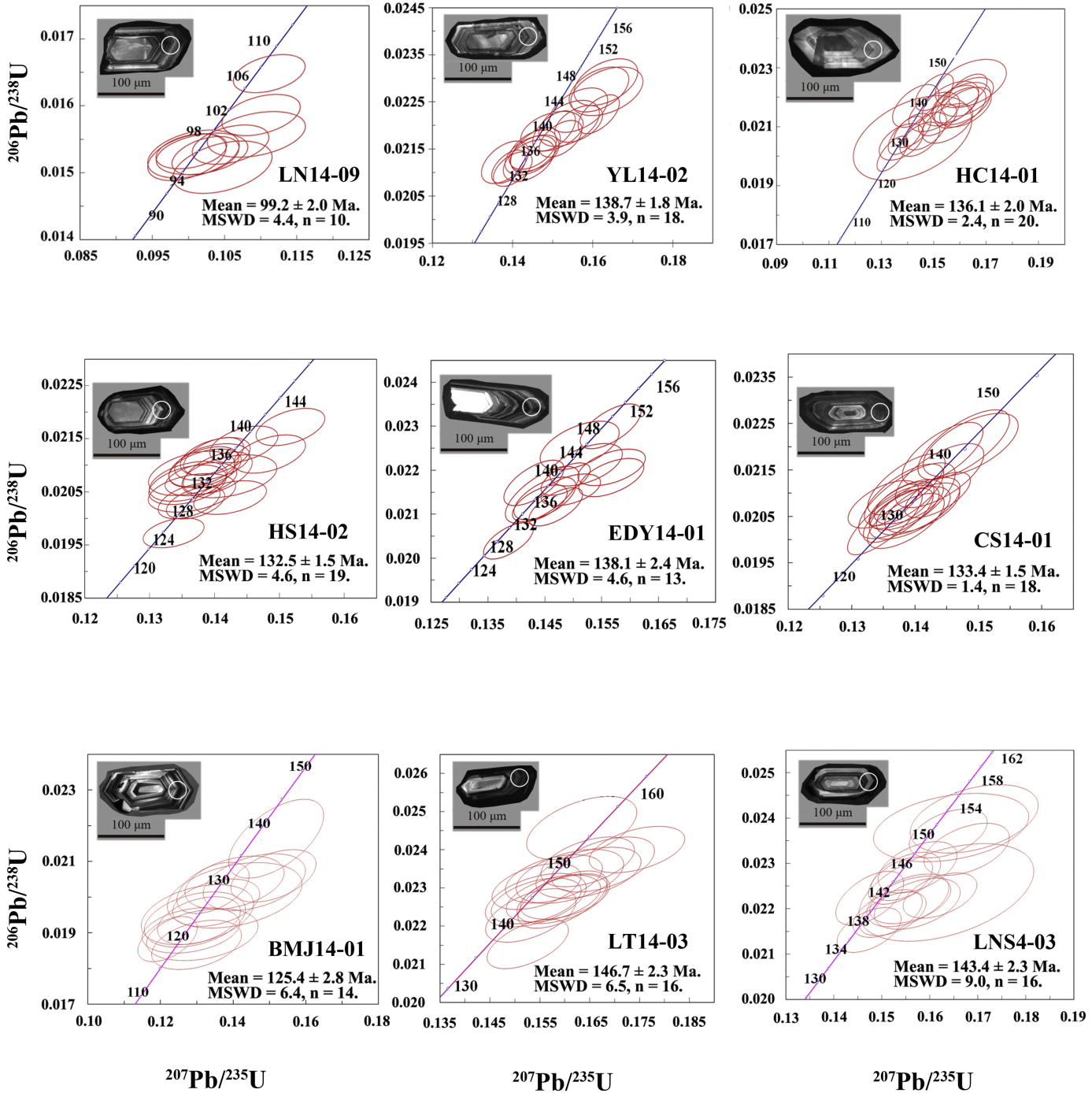
LN14-09
Mean = 99.2 ± 2.0 Ma.
MSWD = 4.4, n = 10.
YL14-02
Mean = 138.7 ± 1.8 Ma.
MSWD = 3.9, n = 18.
HC14-01
Mean = 136.1 ± 2.0 Ma.
MSWD = 2.4, n = 20.
HS14-02
Mean = 132.5 ± 1.5 Ma.
MSWD = 4.6, n = 19.
EDY14-01
Mean = 138.1 ± 2.4 Ma.
MSWD = 4.6, n = 13.
CS14-01
Mean = 133.4 ± 1.5 Ma.
MSWD = 1.4, n = 18.
BMJ14-01
Mean = 125.4 ± 2.8 Ma.
MSWD = 6.4, n = 14.
LT14-03
Mean = 146.7 ± 2.3 Ma.
MSWD = 6.5, n = 16.
LNS4-03
Mean = 143.4 ± 2.3 Ma.
MSWD = 9.0, n = 16.
100 μm
$^{206}Pb/^{238}U$
$^{207}Pb/^{235}U$

Figure 3

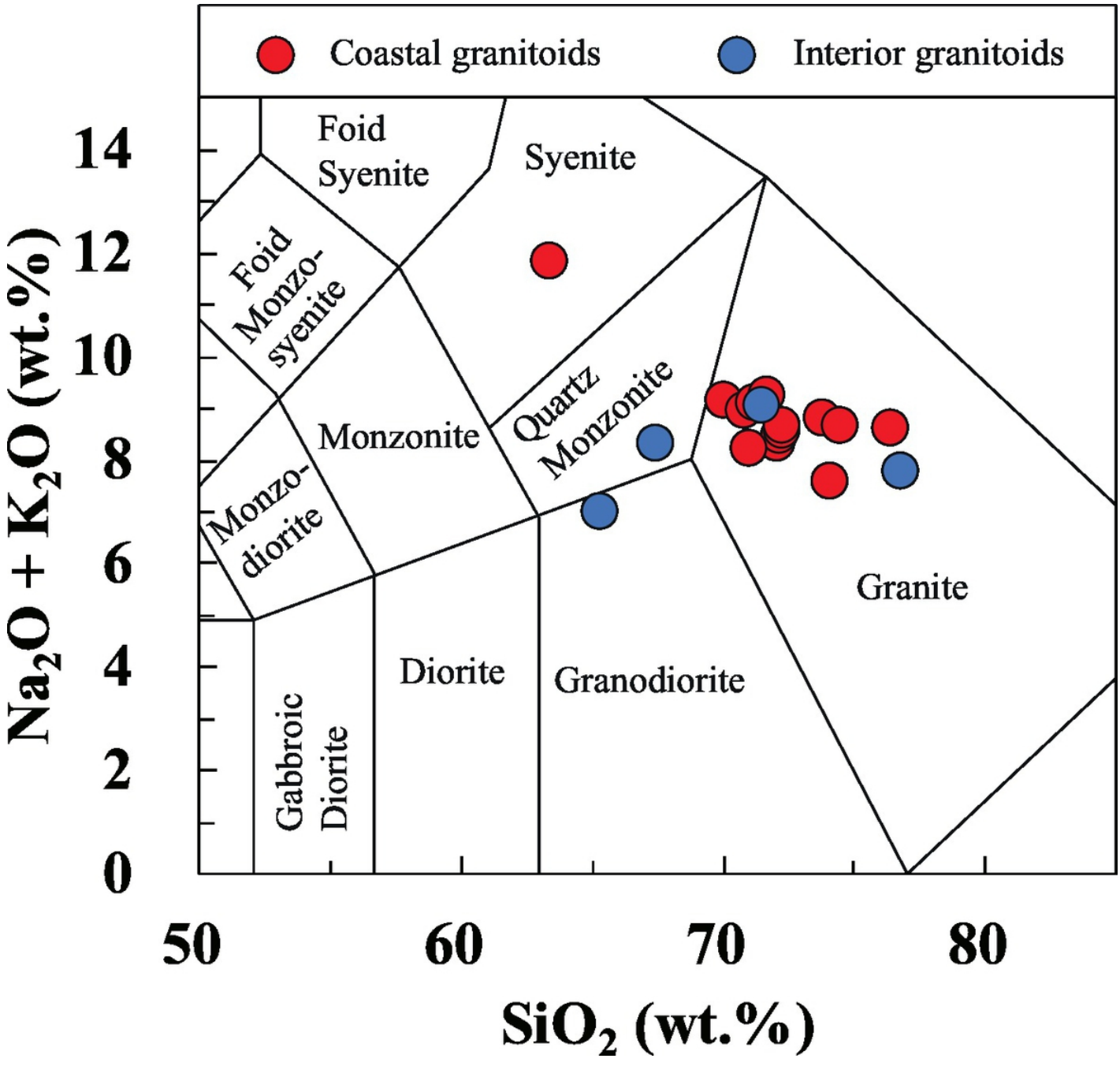
Coastal granitoids
Interior granitoids
Foid Syenite
Syenite
Foid Monzo-syenite
Monzonite
Quartz Monzonite
Monzo-diorite
Granite
Gabbroic Diorite
Diorite
Granodiorite
14
12
10
8
6
4
2
0
50
60
70
80
$Na_2O + K_2O$ (wt.%)
$SiO_2$ (wt.%)

Figure 4

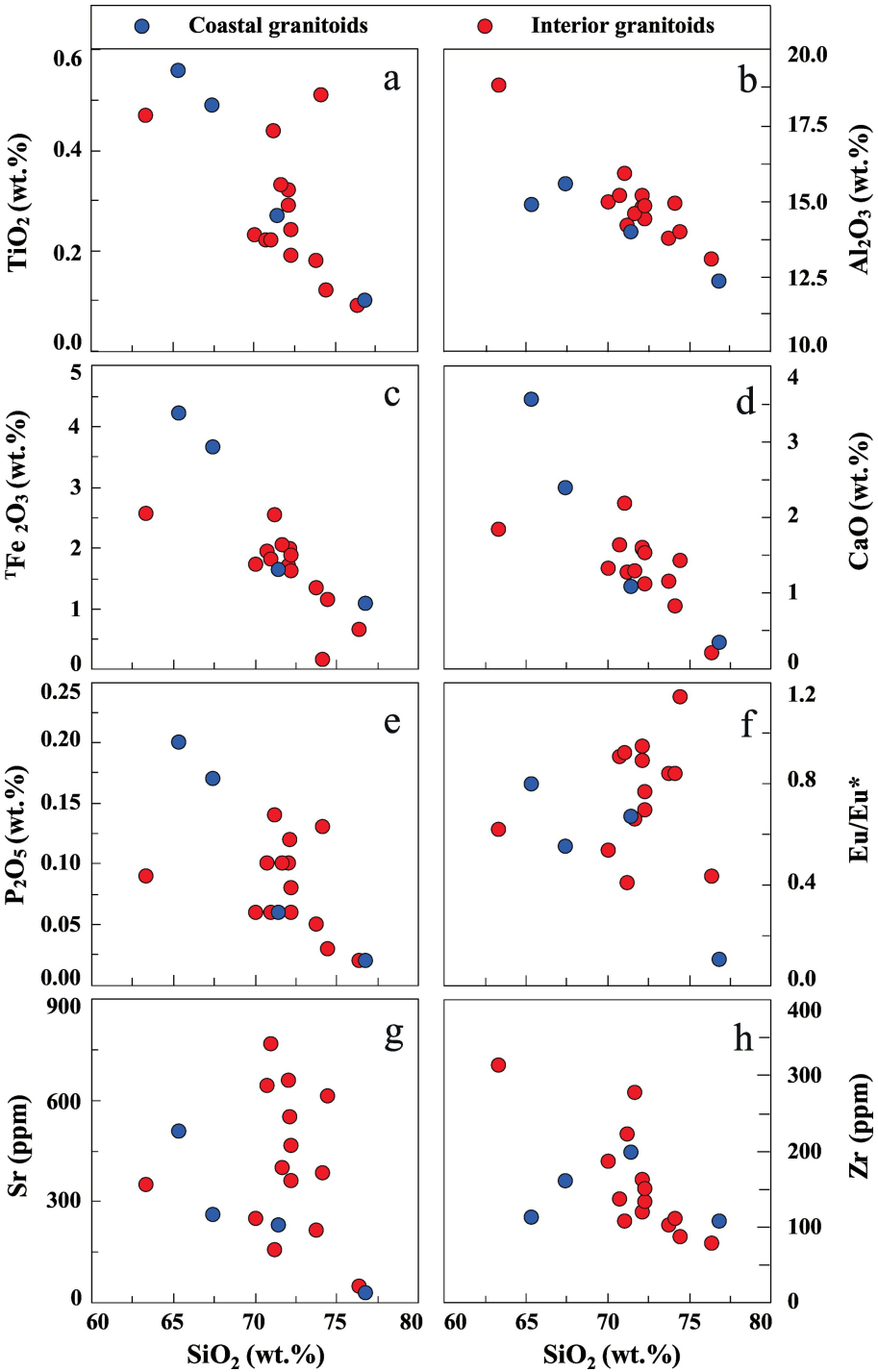
Coastal granitoids
Interior granitoids
a
b
c
d
e
f
g
h
TiO2 (wt.%)
Al2O3 (wt.%)
TFe2O3 (wt.%)
CaO (wt.%)
P2O5 (wt.%)
Eu/Eu*
Sr (ppm)
Zr (ppm)
SiO2 (wt.%)
SiO2 (wt.%)

Figure 5

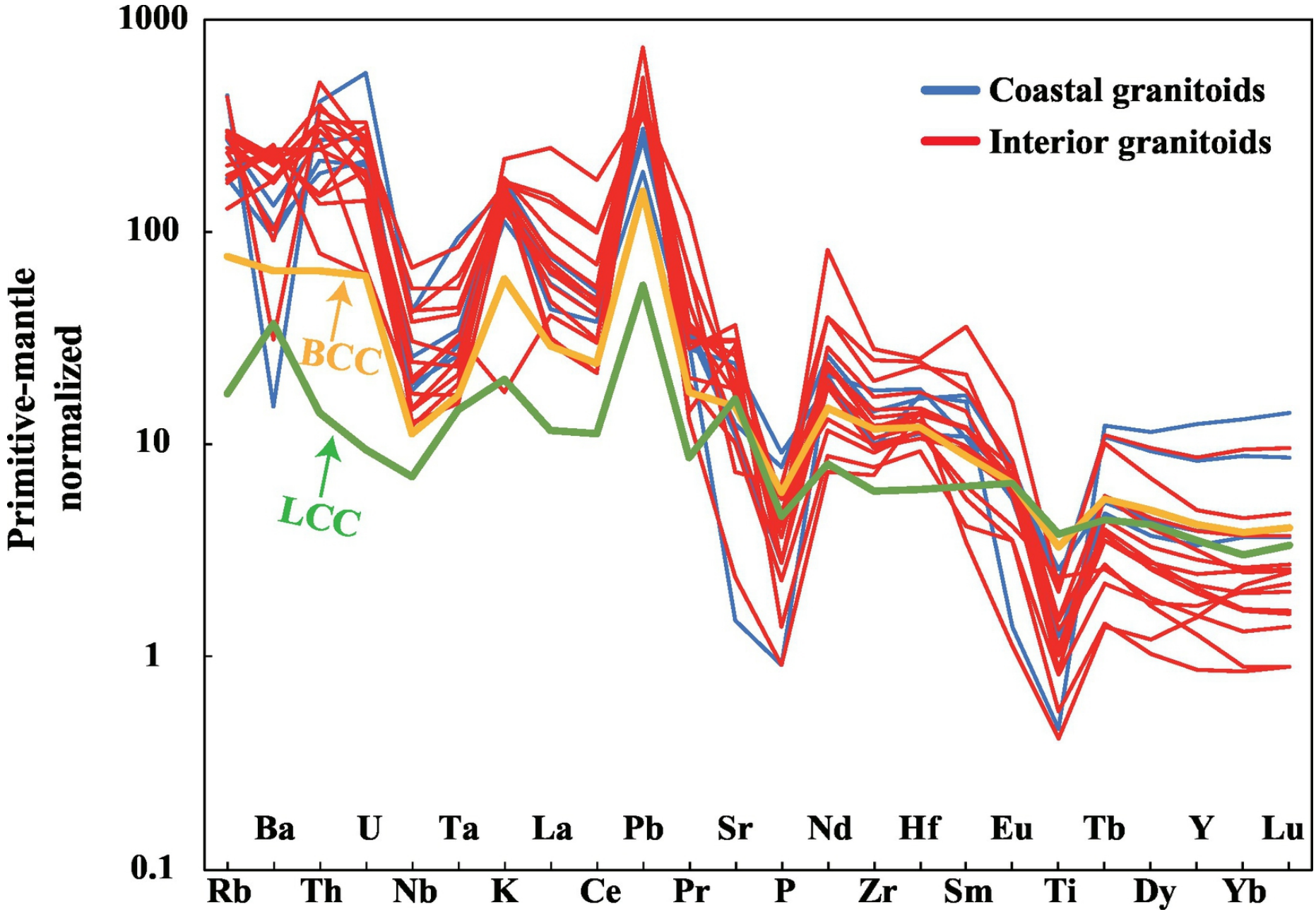
1000
100
10
1
0.1
Primitive-mantle normalized
Coastal granitoids
Interior granitoids
BCC
LCC
Ba
U
Ta
La
Pb
Sr
Nd
Hf
Eu
Tb
Y
Lu
Rb
Th
Nb
K
Ce
Pr
P
Zr
Sm
Ti
Dy
Yb

Figure 6

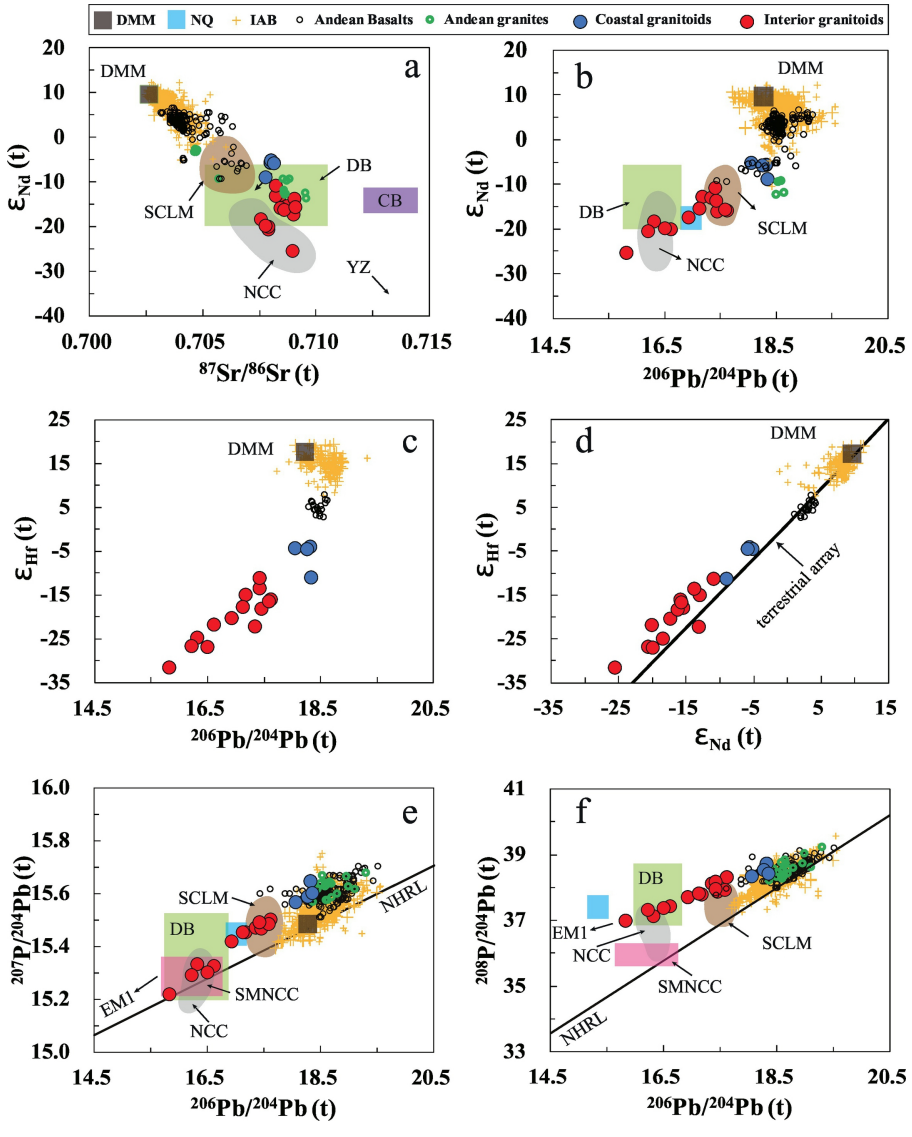
DMM
NQ
IAB
Andean Basalts
Andean granites
Coastal granitoids
Interior granitoids
a
b
c
d
e
f
DMM
SCLM
DB
CB
NCC
YZ
terrestrial array
SMNCC
EM1
NHRL
$\varepsilon_{Nd}$ (t)
$^{87}Sr/^{86}Sr$ (t)
$^{206}Pb/^{204}Pb$ (t)
$\varepsilon_{Hf}$ (t)
$^{207}P/^{204}Pb$ (t)
$^{208}P/^{204}Pb$ (t)

Figure 7

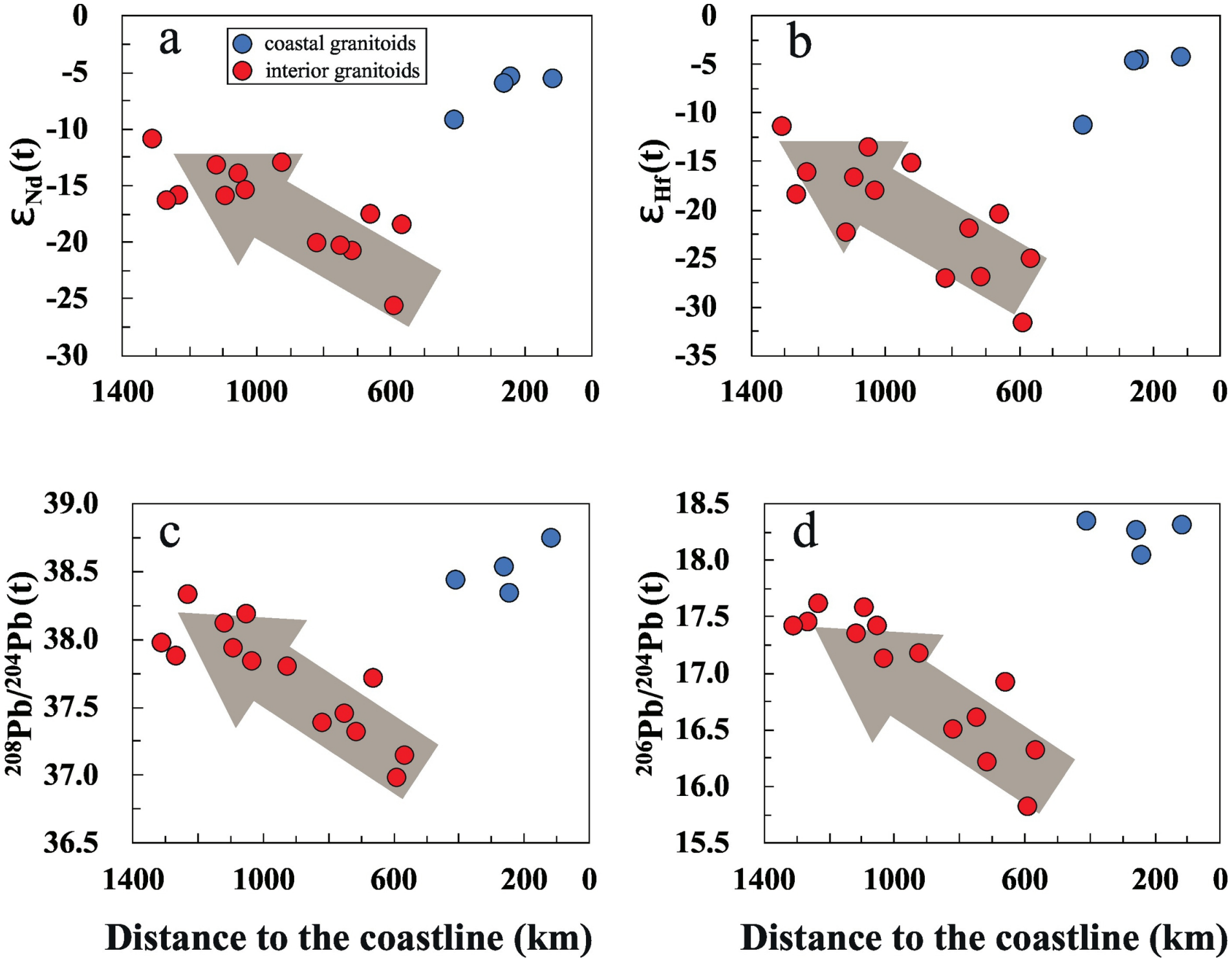
a
coastal granitoids
interior granitoids
$\varepsilon_{Nd}(t)$
0
-5
-10
-15
-20
-25
-30
b
$\varepsilon_{Hf}(t)$
0
-5
-10
-15
-20
-25
-30
-35
c
$^{208}Pb/^{204}Pb\ (t)$
39.0
38.5
38.0
37.5
37.0
36.5
d
$^{206}Pb/^{204}Pb\ (t)$
18.5
18.0
17.5
17.0
16.5
16.0
15.5
1400
1000
600
200
0
Distance to the coastline (km)

Figure 8

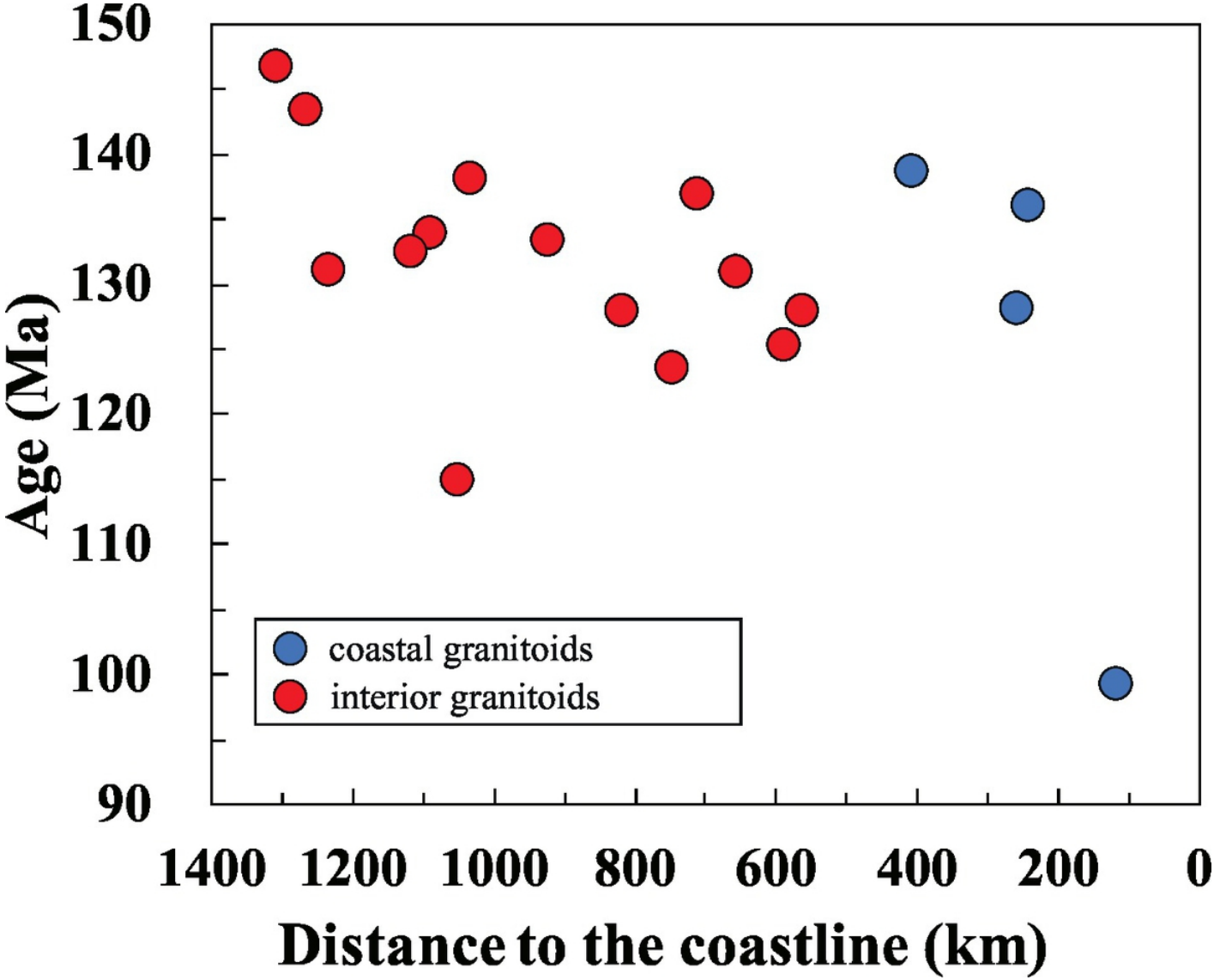
150
140
130
120
110
100
90
Age (Ma)
1400
1200
1000
800
600
400
200
0
Distance to the coastline (km)
coastal granitoids
interior granitoids

Figure 9

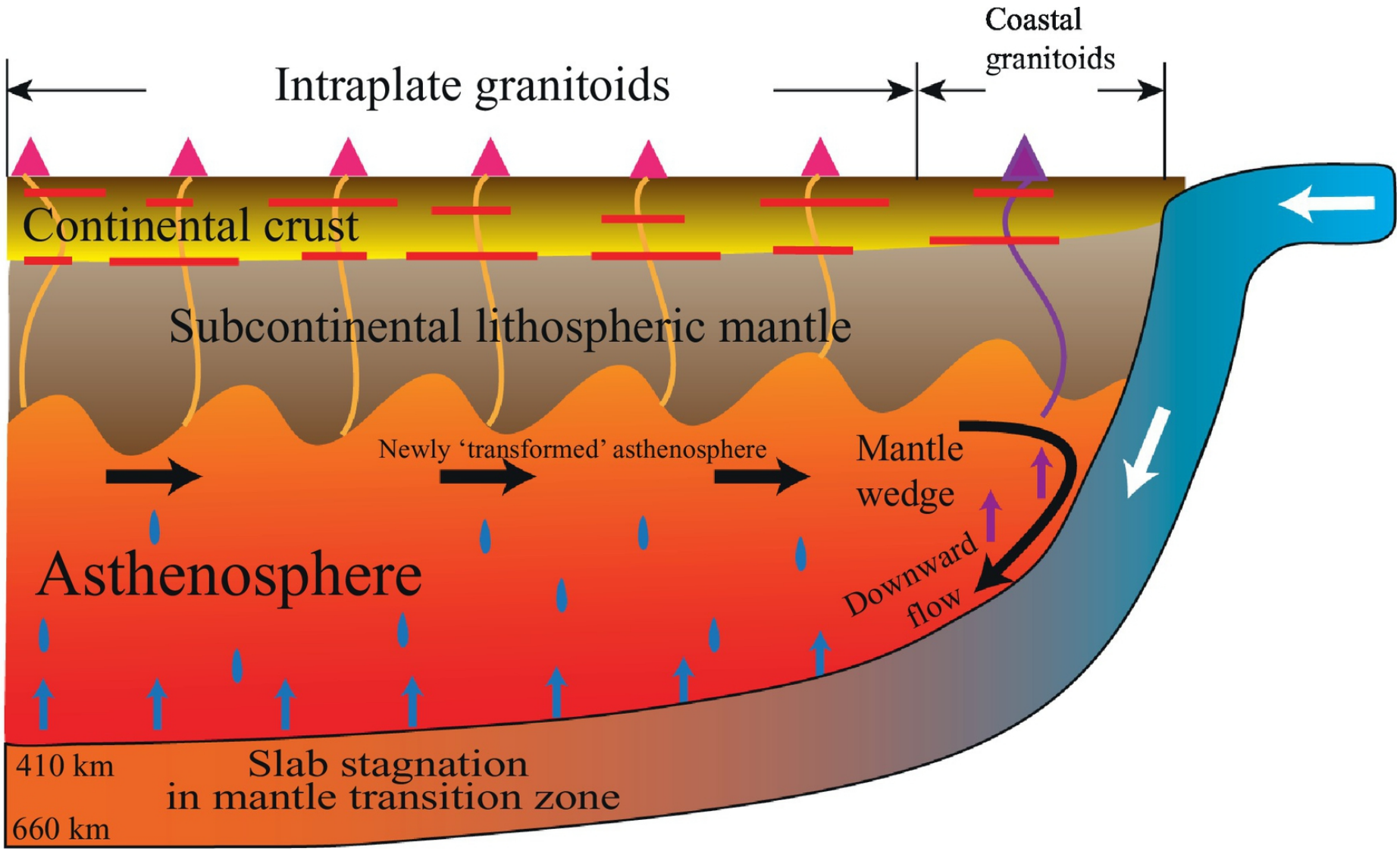
Coastal
granitoids
Intraplate granitoids
Continental crust
Subcontinental lithospheric mantle
Newly 'transformed' asthenosphere
Mantle
wedge
Asthenosphere
Downward
flow
410 km
Slab stagnation
in mantle transition zone
660 km

Figure 10